THIRD QUARTERLY REPORT

Thin-Film Personal Communications and Telemetry System (TFPCTS)

Contract No. NAS 9-3924

Submitted to

NATIONAL AERONAUTICS AND SPACE ADMINISTRATION
MANNED SPACECRAFT CENTER
Houston, Texas

MELPAR, INC.
7700 Arlington Boulevard
Falls Church, Virginia

Third Quarterly Report

THIN-FILM PERSONAL COMMUNICATIONS AND TELEMETRY SYSTEM (TFPCTS)

For the period of June 21, 1965 to September 21, 1965

Contract No. NAS 9-3924

October 1965

Submitted to

National Aeronautics and Space Administration
Manned Spacecraft Center
Houston, Texas

Submitted by

Melpar, Inc.
7700 Arlington Boulevard
Falls Church, Virginia

TABLE OF CONTENTS

TABLE OF CONTENTS (Continued)

LIST OF ILLUSTRATIONS

LIST OF ILLUSTRATIONS (Continued)

LIST OF TABLES

1. INTRODUCTION

This Third Quarterly Report is submitted in compliance with Contract NAS 9-3924. Phase A of this contract is a research effort to develop thin-film active devices and passive circuit elements for use at ultrahigh frequencies. The thin-film components will be used in the design of a Thin-Film Personal Communications and Telemetry System (TFPCTS) in monotronic form.

At this time, there have been no unexpected problems or delays. Work is progressing smoothly in accordance with the PERT time table, which is presented in an up-to-date version at this nine-month point in phase A. The revised PERT Chart has the appropriate bubbles shaded to indicate approximately the various states of completion of each task.

During the third quarter, the Inductor Investigation and High-permeability Films Investigation were concluded. The work effort had been increased on both of these research tasks to complete various phases of the investigations which, otherwise, could not have been completed. The thin-film inductors formed under this contract have proved practical, and are included with the other passive components as available for use in the TFPCTS. Ferrite films were formed in vacuo using standard vacuum-deposition techniques for the first time under this contract. That is, no other report of this accomplishment has come to the attention of this laboratory. However, it will require further development, beyond the scope of this contract, before this thin-film material can be optimized for circuit use.

One of the main objectives of this program is the development of a high-frequency active device. Methods of forming potential high-frequency

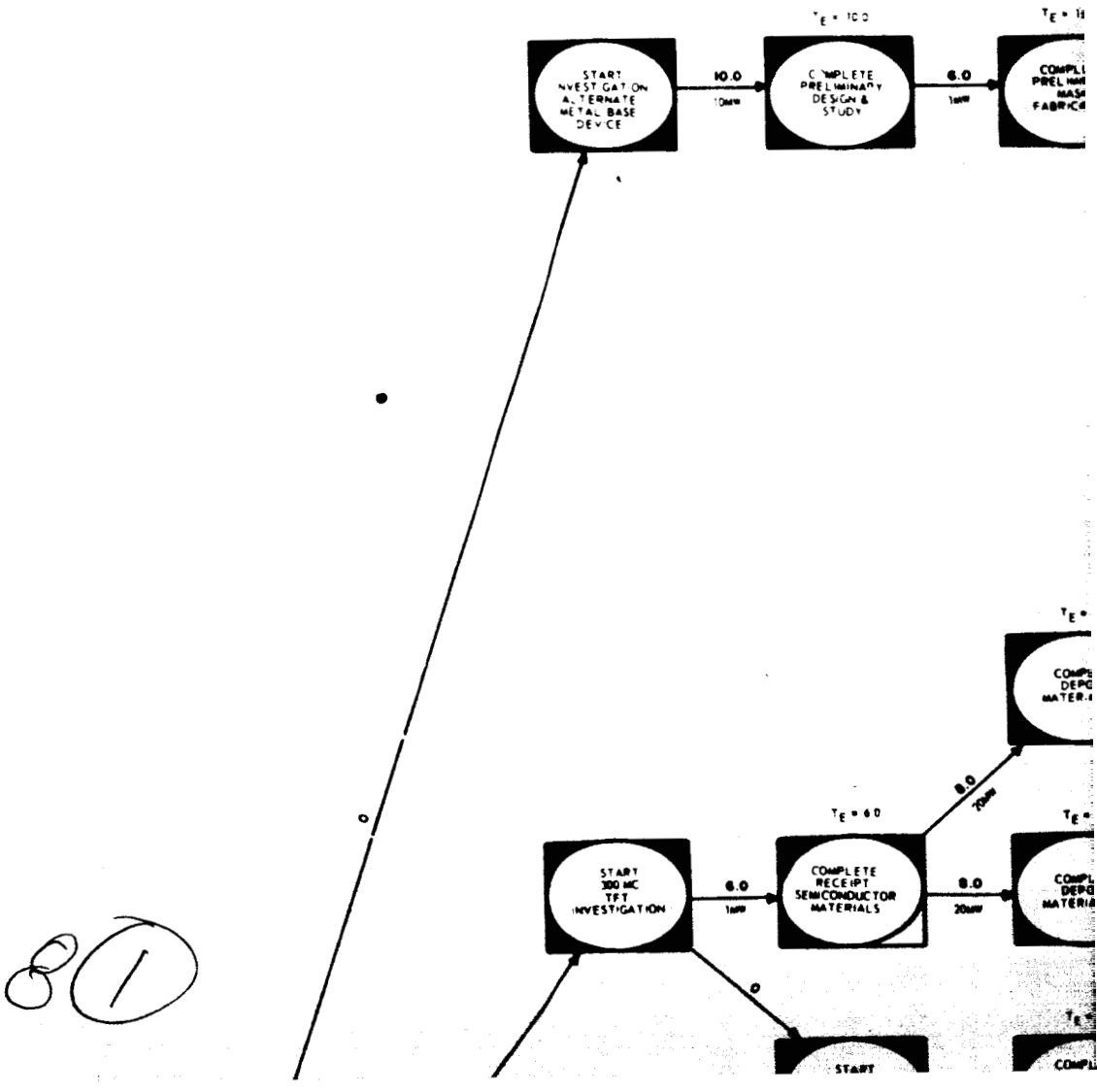
START INVESTIGATION ALTERNATE METAL BASE DEVICE
10.0
10MM
COMPLETE PRELIMINARY DESIGN & STUDY
6.0
1MM
START 300 MC TFT INVESTIGATION
6.0
1MM
COMPLETE RECEIPT SEMICONDUCTOR MATERIALS
8.0
20MM

81

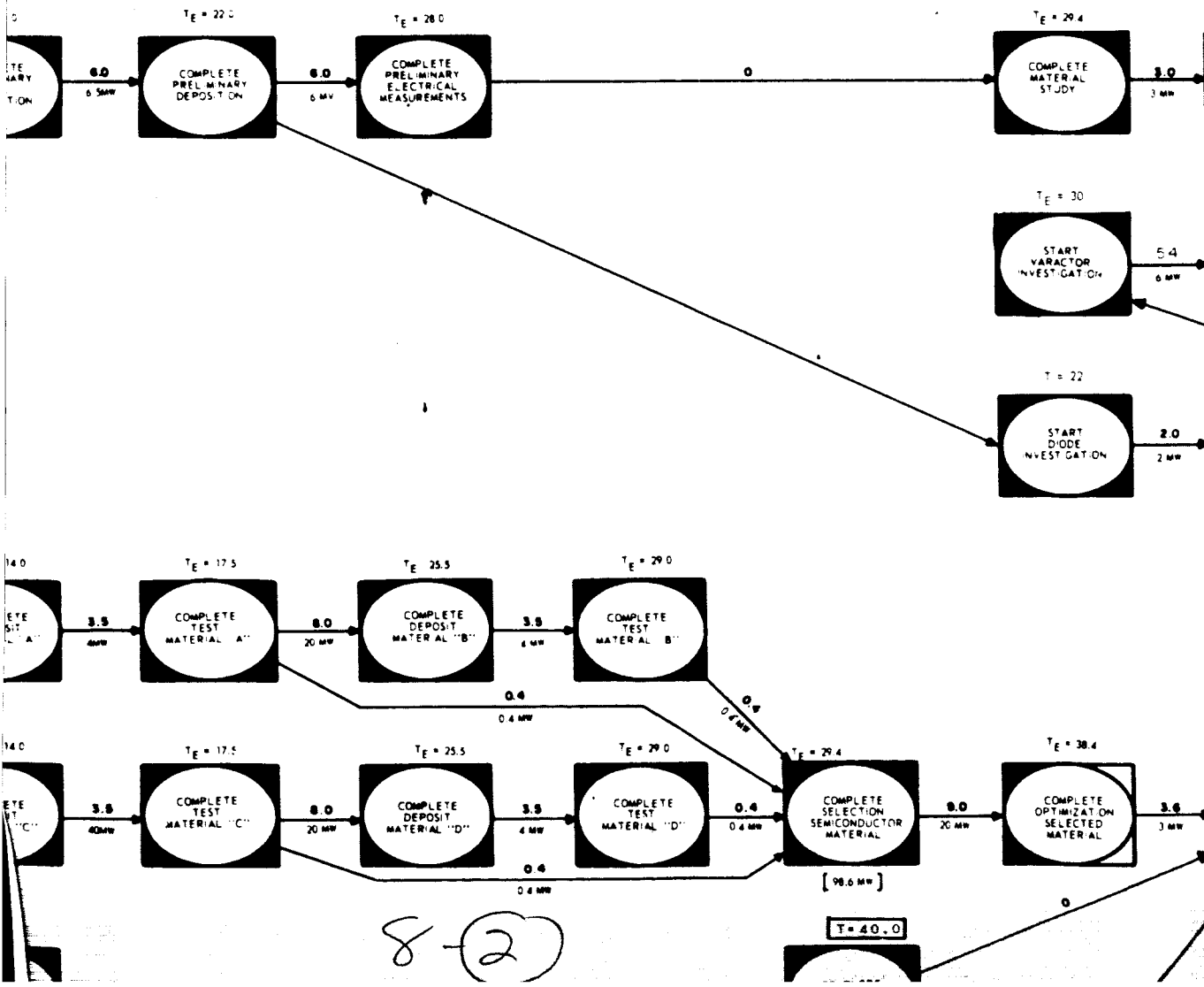
T_E = 22.0
T_E = 28.0
T_E = 29.4
6.0
6 Sww
COMPLETE PRELIMINARY DEPOSITION
6.0
6 MW
COMPLETE PRELIMINARY ELECTRICAL MEASUREMENTS
0
COMPLETE MATERIAL STUDY
3.0
3 MW
T_E = 30
START VARACTOR INVESTIGATION
5.4
6 MW
T = 22
START DIODE INVESTIGATION
2.0
2 MW
T_E = 17.5
T_E 25.5
T_E = 29.0
3.5
COMPLETE TEST MATERIAL "A"
6.0
20 MW
COMPLETE DEPOSIT MATERIAL "B"
3.5
6 MW
COMPLETE TEST MATERIAL "B"
0.4
0.4 MW
0.4
0.4 MW
T_E = 17.5
T_E = 25.5
T_E = 29.0
T_E = 29.4
T_E = 38.4
3.5
COMPLETE TEST MATERIAL "C"
6.0
20 MW
COMPLETE DEPOSIT MATERIAL "D"
3.5
4 MW
COMPLETE TEST MATERIAL "D"
0.4
0.4 MW
COMPLETE SELECTION SEMICONDUCTOR MATERIAL
[98.6 MW]
6.0
20 MW
COMPLETE OPTIMIZATION SELECTED MATERIAL
3.6
3 MW
0.4
0.4 MW
T = 40.0
0

8-(2)

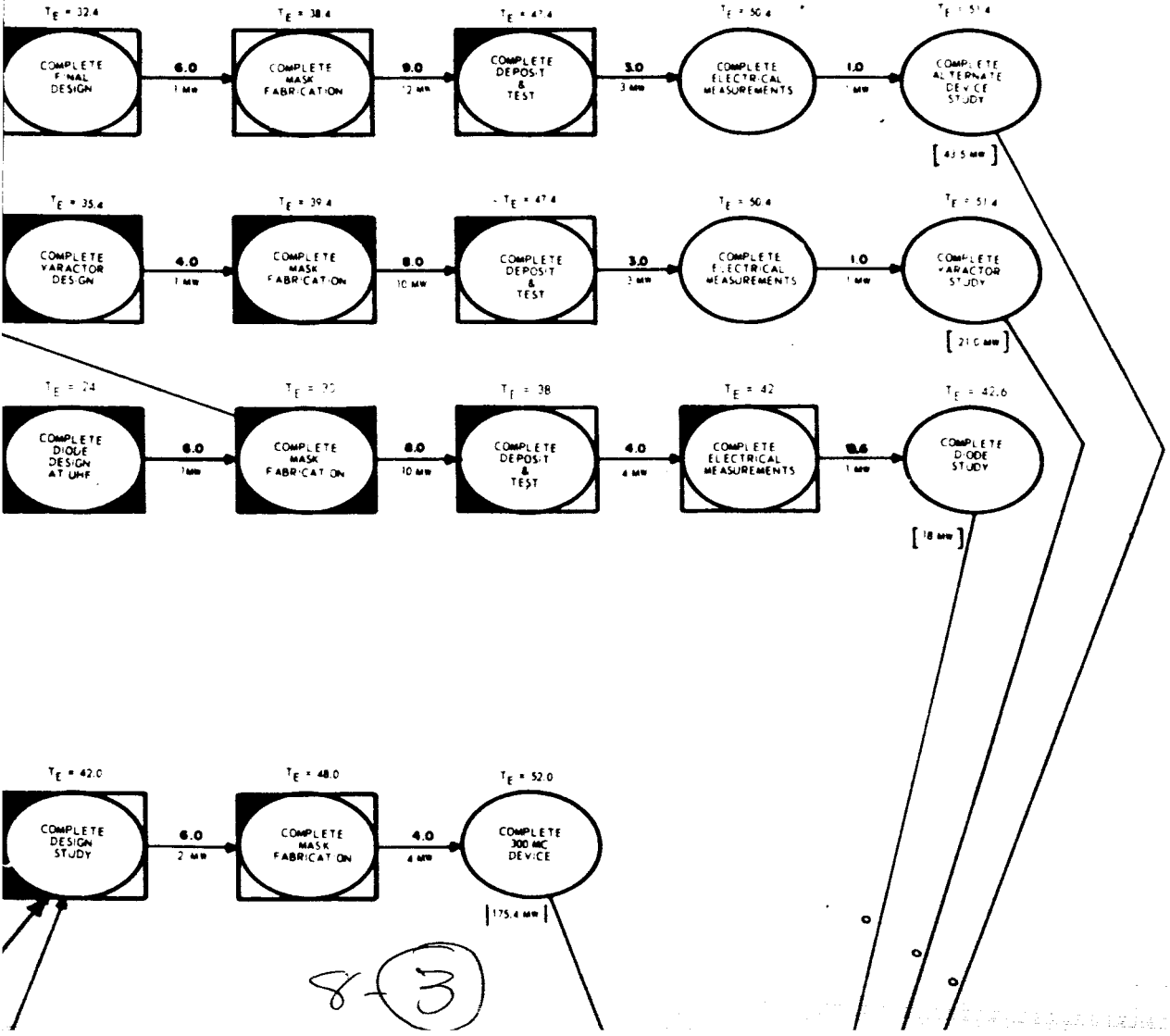
T_E = 32.4
COMPLETE FINAL DESIGN
6.0
1 MW
T_E = 38.4
COMPLETE MASK FABRICATION
9.0
12 MW
T_E = 47.4
COMPLETE DEPOSIT & TEST
3.0
3 MW
T_E = 50.4
COMPLETE ELECTRICAL MEASUREMENTS
1.0
1 MW
T_E = 51.4
COMPLETE ALTERNATE DEVICE STUDY
[43.5 MW]
T_E = 35.4
COMPLETE VARACTOR DESIGN
4.0
1 MW
T_E = 39.4
COMPLETE MASK FABRICATION
8.0
10 MW
T_E = 47.4
COMPLETE DEPOSIT & TEST
3.0
3 MW
T_E = 50.4
COMPLETE ELECTRICAL MEASUREMENTS
1.0
1 MW
T_E = 51.4
COMPLETE VARACTOR STUDY
[21.0 MW]
T_E = 24
COMPLETE DIODE DESIGN AT UHF
6.0
1 MW
T_E = 30
COMPLETE MASK FABRICATION
8.0
10 MW
T_E = 38
COMPLETE DEPOSIT & TEST
4.0
4 MW
T_E = 42
COMPLETE ELECTRICAL MEASUREMENTS
1.6
1 MW
T_E = 42.6
COMPLETE DIODE STUDY
[18 MW]
T_E = 42.0
COMPLETE DESIGN STUDY
6.0
2 MW
T_E = 48.0
COMPLETE MASK FABRICATION
4.0
4 MW
T_E = 52.0
COMPLETE 300 MC DEVICE
175.4 MW

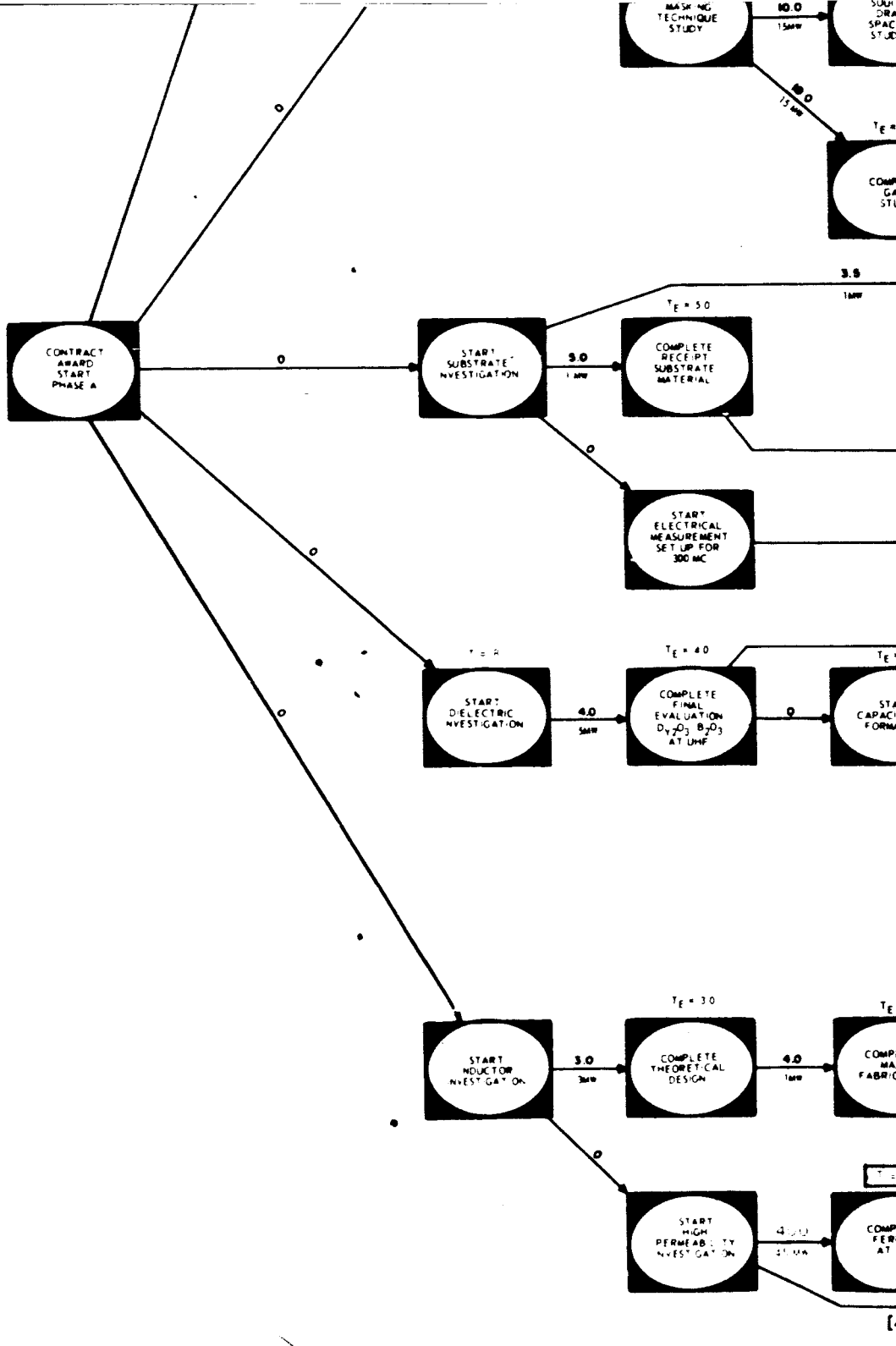
MASKING TECHNIQUE STUDY
10.0
15 MAY
CONTRACT AWARD START PHASE A
0
START SUBSTRATE INVESTIGATION
3.0
1 NOV
T_E = 50
COMPLETE RECEIPT SUBSTRATE MATERIAL
3.5
1 NOV
START ELECTRICAL MEASUREMENT SET UP FOR 300 MC
START DIELECTRIC INVESTIGATION
4.0
5 NOV
T_E = 40
COMPLETE FINAL EVALUATION $D_{Y_2O_3}$ $B_{Y_2O_3}$ AT UMF
9
START INDUCTOR INVESTIGATION
3.0
3 NOV
T_E = 30
COMPLETE THEORETICAL DESIGN
4.0
1 NOV
START HIGH PERMEABILITY INVESTIGATION

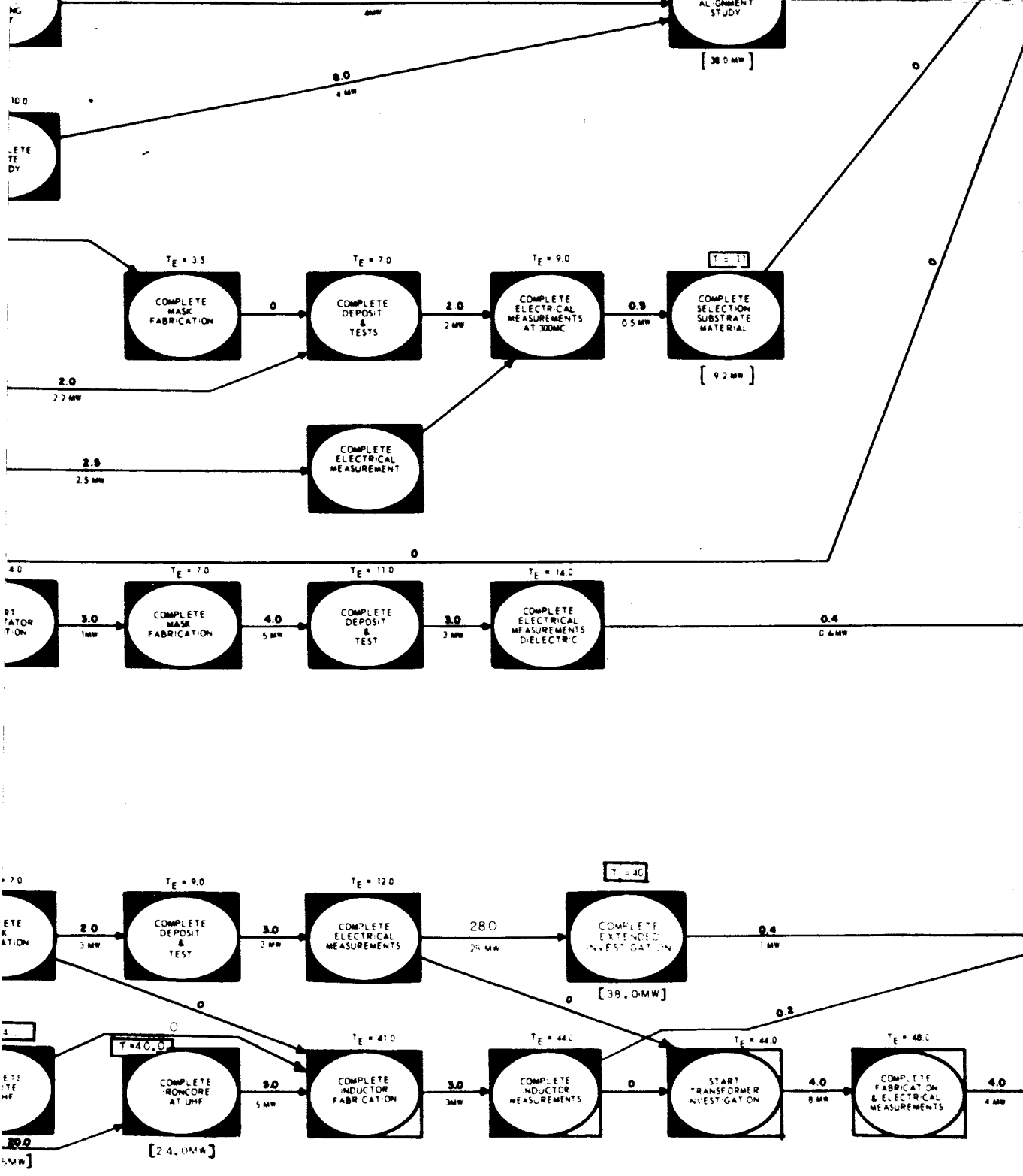
8.0
4 MW
[38.0 MW]
T_E = 3.5
COMPLETE MASK FABRICATION
0
T_E = 7.0
COMPLETE DEPOSIT & TESTS
2.0
2 MW
T_E = 9.0
COMPLETE ELECTRICAL MEASUREMENTS AT 300MC
0.5
0.5 MW
T = 11
COMPLETE SELECTION SUBSTRATE MATERIAL
[9.2 MW]
2.0
2.2 MW
2.5
2.5 MW
COMPLETE ELECTRICAL MEASUREMENT
0
T_E = 7.0
3.0
1 MW
COMPLETE MASK FABRICATION
4.0
5 MW
T_E = 11.0
COMPLETE DEPOSIT & TEST
3.0
3 MW
T_E = 14.0
COMPLETE ELECTRICAL MEASUREMENTS DIELECTRIC
0.4
0.4 MW
T_E = 9.0
2.0
3 MW
COMPLETE DEPOSIT & TEST
3.0
3 MW
T_E = 12.0
COMPLETE ELECTRICAL MEASUREMENTS
280
28 MW
T = 40
COMPLETE EXTENDED INVESTIGATION
0.4
1 MW
[38.0MW]
0
0
0.2
T = 40.0
COMPLETE IRONCORE AT UHF
3.0
5 MW
[24.0MW]
T_E = 41.0
COMPLETE INDUCTOR FABRICATION
3.0
3MW
T_E = 44.0
COMPLETE INDUCTOR MEASUREMENTS
0
T_E = 44.0
START TRANSFORMER INVESTIGATION
4.0
8 MW
T_E = 48.0
COMPLETE FABRICATION & ELECTRICAL MEASUREMENTS
4.0
4 MW

8-5

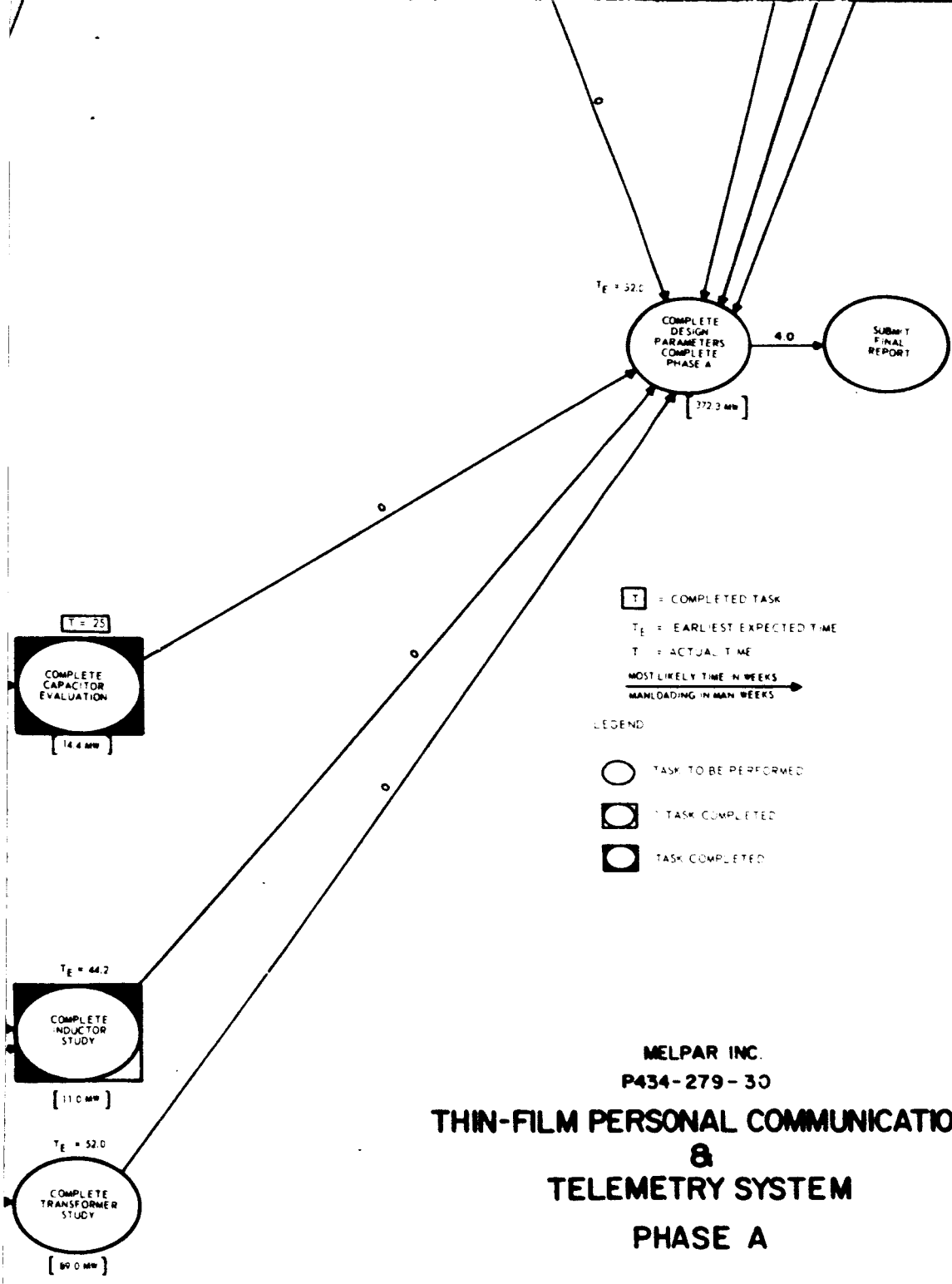

MELPAR INC.

P434-279-30

THIN-FILM PERSONAL COMMUNICATION & TELEMETRY SYSTEM PHASE A

8-6

thin-film triodes have been achieved and are in the process of being employed. These masking advancements are discussed in this report; however, they are too recent to have undergone complete frequency tests. The work of optimizing the selected semiconductor materials, cadmium selenide, cadmium sulfide, cadmium telluride and tellurium, is continuing. The formation of a metal-base transistor is presently being attempted. The junctions which will be used to form the transistor have been very promising. These junctions, which are a technological discovery of this program and have been developing at a surprisingly fast pace, are now being used in an attempt to form high-frequency diodes and varactors. A section on circuit design has been added to this report. Since the inception of this contract, electrical engineers have been studying the design approaches and circuit-component requirements for a monotronic TFPCTS. Preliminary circuit passive component requirements are presented and discussed. Also, a brochure, "Thin-Film Circuits," which presents the state of the art of thin-film passive components in detail, is included as an appendix to this report.

The following sections contain detailed accounts of the aforementioned work.

2. HIGH-FREQUENCY THIN-FILM TRIODES

2.1 High-Frequency Measurements

Aside from film and device studies utilizing CdTe (doped and undoped), most of the effort this quarter has been that of forming CdSe or Te devices.

Measurements of CdSe triodes (See paragraph 2.4) formed this quarter resulted in gain band widths (GBW) to 10.8 mcs, while Te devices exhibited a GBW of up to 10 mcs. These measured values where about one-half that calculated from the conditional approximate equation

$$GBW = \frac{gm}{2\pi C}$$

using measured values of C and gm.

Although the frequency capabilities measured thus far have been low for the ultimate requirements of this contract, it was very encouraging to note that the devices tested utilize rather large (1.0-mil wide) gate electrodes. The Te devices also indicated up to 200 mw capability.

During the last phase of this quarter, an effort to reduce the gate-electrode width was very successful. Gate widths have been reduced to that of the smallest source-drain spacings of 2.5 microns (0.1 mil). However, the technique has not been applied as yet to devices of which a GBW has been measured. It is expected that, with the reduced gate-electrode area, a notable improvement of frequency capability will be noted.

2.2 Electrode Masking Techniques

2.2.1 Source-Drain Spacing

Figure 1 illustrates the basic arrangement used in attaching fine tungsten wires to an etched molybdenum mask to form the source-drain electrodes.

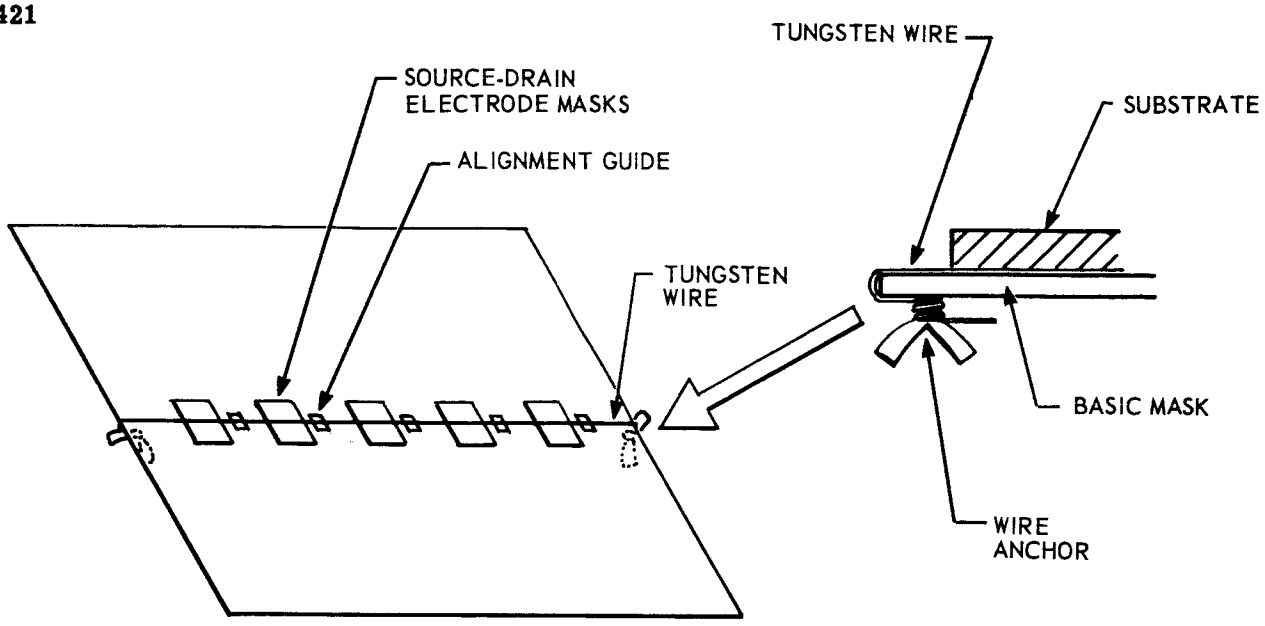

Figure 1. Basic Source-drain Mask

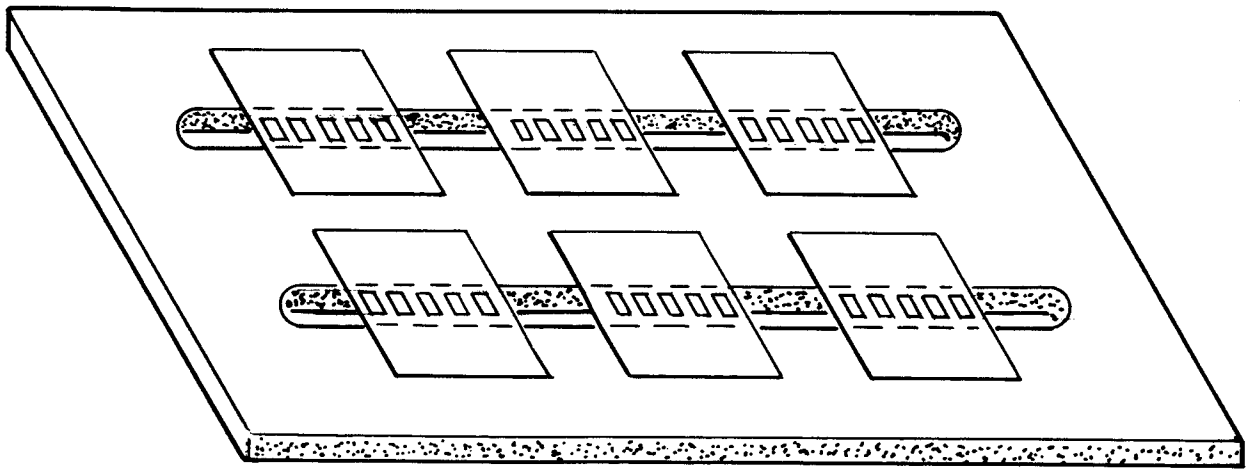

Figure 2. Source-drain Mask Support

The wire acts to form the spacing between a metal deposit to form the separate electrodes. Although a five-device arrangement is shown for clarity, this basic method is also used in forming more numerous multirow device layouts.

As a visual aid (not necessarily required), an alignment deposition is evaporated simultaneously with the source-drain electrodes. This small slit (indicated in figure 1) is used to optically align the latter gate-electrode deposition with the source-drain spacing.

Figure 2 is a sketch of the type of support utilized for a source-drain deposition to be made on several substrates at a time. (This support is also used for the gate evaporation.) Weights (copper bars) are placed on the substrates to ensure intimate contact of the substrate to the mask. It is necessary that the tungsten wire (or wires) be tight to ensure a straight-line separation of electrodes, especially important when aligning the gate electrode.

Figure 3 is a photograph of the vacuum system interior arrangement for the deposition of source-drain electrodes. A quartz heater lamp housing astride the copper bars (weights on the substrates) provides heat for outgassing and deposition. Substrates (Corning 10-mil 0211) are heated to 400°C for outgassing and then cooled to approximately 250° for the deposition. In this picture, the substrates and masks are obscured by the wieghts and mask supports.

By using the fine wire attached to basic molybdenum mask technique, it has been found easy to readily and practically produce large numbers of source-drain electrodes with spacings down to 0.1 mil (2.5 microns).

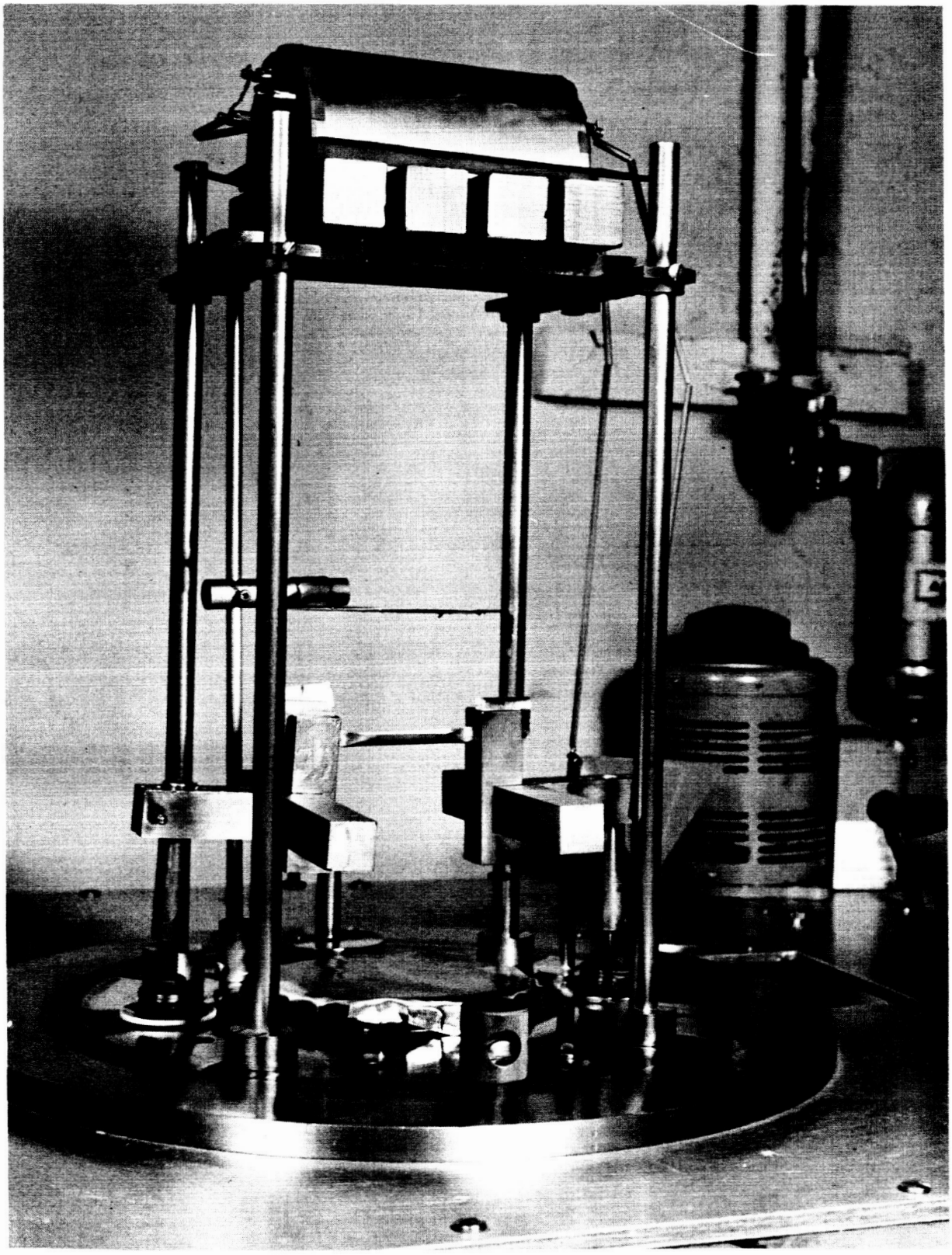

Figure 3. Vacuum System Interior Arrangement for Deposition of Source-drain Electrodes

Nichrome V, or chromium, is the metal used to form the source-drain electrodes. A tungsten boat (10-mil, R.D. Mathis or Allen Jones) is used as the evaporating boat. The durability of this boat for nichrome has been found strongly dependent on the vacuum pressure achieved for evaporation. From four to eight evaporations (0.5 gram per charge) of nichrome can be expected in good vacuum before burnout. Durability of the boat has also been found dependent on frequency of use and evaporation rate. The faster the frequency of use, the better, and, within limits, the faster the deposition, the better.

Figure 4 is a photomicrograph (42X) partially showing the source-drain spacing of 0.1 mil and the alignment guide (also having a 0.1-mil alignment slit) at the bottom of the photograph.

2.2.2 Gate Masking

Four methods of forming a mask capable of resulting in very narrow deposits (gate electrodes) have been attempted. These include:

a. Etching thin metal foils (stainless-steel/nickel or molybdenum) by electrochemical or pure chemical etch.

b. Electroforming nickel masks.

c. Spacing of knife edges (metal foils).

d. Spacing of wires on basic masks.

After considerable effort, the third method has been discontinued. At separations of less than 0.5 mil, it was found that the edge resolution was insufficiently fine to form a well-defined deposit. Other problems, such as an aluminum deposition resulting in brown semiconducting layers, also occcurred below this width in spite of good vacuum and deposition practices.

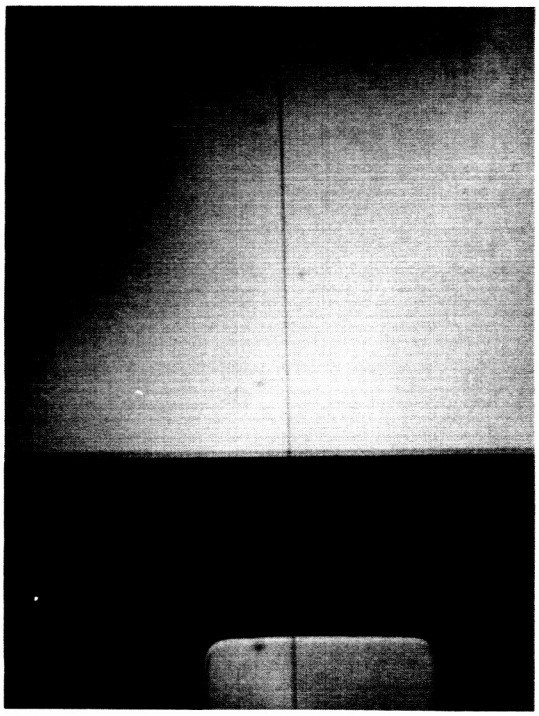

Figure 4. Source-drain Electrode Evaporation (42X)

Although protographic images of 0.2-mil widths have been achieved in the photography, problems thus far exist in method No. 1 because of metal-grain boundaries in the foil and in method No. 2 because of irregularities in the parent base metal. These two methods have not been abandoned, however, because a further polishing of the metals (as purchased) may result in somewhat more success. During the next quarter, effort will be made to reduce the problems involved.

Method No. 4 has been very successful, and has been used to produce very small (2.5-micron) gate widths. Still further reduction of this width is apparently possible because no deterious effects occur with the aluminum deposit (i.e., it is very conductive) in spite of the deposit through the very narrow aperture. Figure 5 illustrates the basic gate mask. Two tungsten wires (1-mil diameter) are attached, side by side, to the basic mask in a manner similar to the single wire forming the source-drain electrodes (see figure 1). Separation of the wires outlining the gate electrode is accomplished either by a spacing wire or a natural lay whereby separation is maintained by tension of the wires. Again, good tension is required to align with the source-drain spacing. Alignment is doen optically by alignment of the gate electrode with the alignment deposition made as a companion with the source-drain electrodes (see figure 4). Figure 6 is a photomicrograph (240X) of a gate electrode formed using this method. The two dark areas straddling the gate electrode are shadows of the two 1-mil wires used to define the aperture. As can be seen, the gate electrode is no greater than 0.2 mils in width. Compared with the photomicrograph of figure 7 (also 240X) of an etched mask of approximately 1.5 mils, a marked improvement is noted.

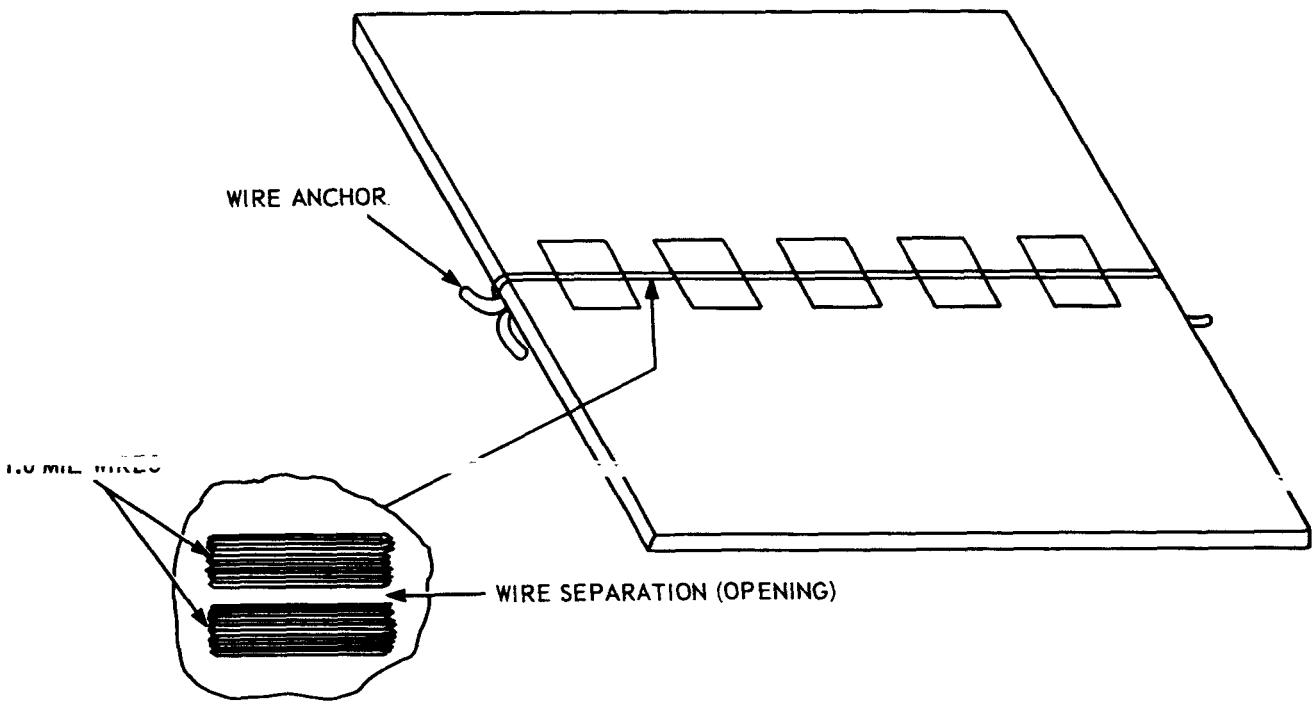

Figure 5. Gate Electrode Masking (Method 4)

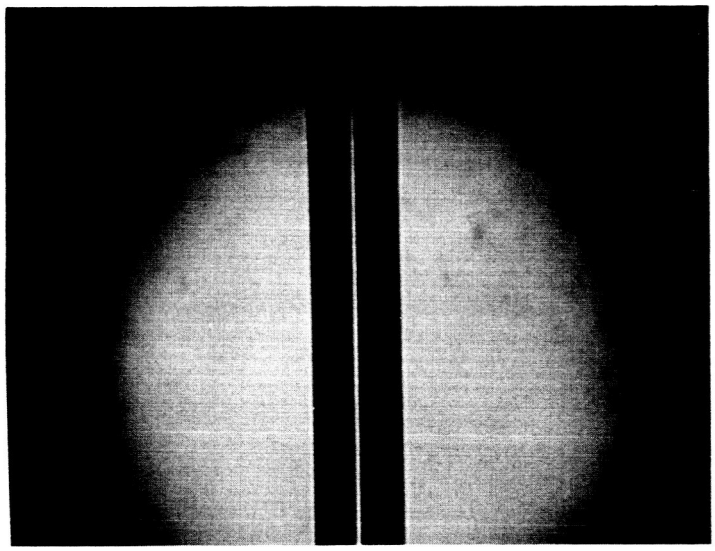

Figure 6. Photomicrograph (240X) of Gate Electrode Formed by Method 4

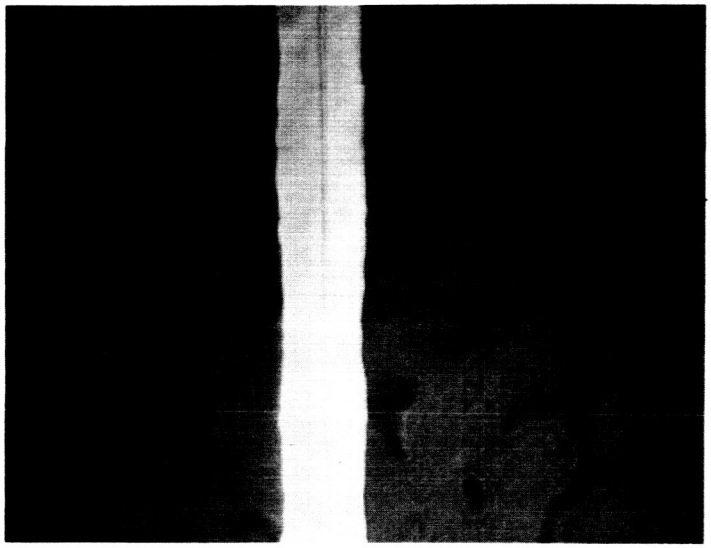

Figure 7. Photomicrograph (240X) of Gate Electrode Formed by Method 1

2.3 Dielectric Depositions

The dielectric used as the insulator layer in thin-film triodes this quarter was primarily SiO. To increase the dielectric breakdown strength, some experiments were performed utilizing mixtures of SiO and boron trioxide (B_2O_3). The deposition is performed at a rather rapid rate (>100Å/sec). Generally, the procedure used is the same as that described in previous quarters.

2.4 Semiconductor Depositions

The techniques described in the first and second quarterly reports were utilized for CdSe and Te deposits. A concentrated effort was conducted on the studies of CdTe films this quarter.

2.4.1 Cadmium Telluride

During the last quarter, the electrical properties of CdTe films and CdTe films doped with indium and iodine, prepared by vacuum evaporation of the compound or vacuum coevaporation of the compound and dopant, were studied. TFTs using CdTe, CdTe(In), and CdTe(I) were fabricated. Transconductances of 10 μ mho or less were observed for CdTe and CdTe(I) TFTs, but transconductances of 1000 μ mhos were attained for CdTe(In) TFTs.

The curve of log of resistance versus reciprocal of absolute temperature for a high-purity CdTe film is shown in figure 8. The film resistance is completely reversible over the range from 25° to 250°C. Above the temperature of 250°C, an irreversible change occurs to the resistance. According to Ichimiya,[1] this is probably due to the selective evaporation of Cd from the surface. Intrinsic conduction is observed above the temperature of 110°C and the slope of the resistance curve shows a main band gap of 1.44 ev. This is in good agreement with the accepted value for CdTe.[1,2,3]

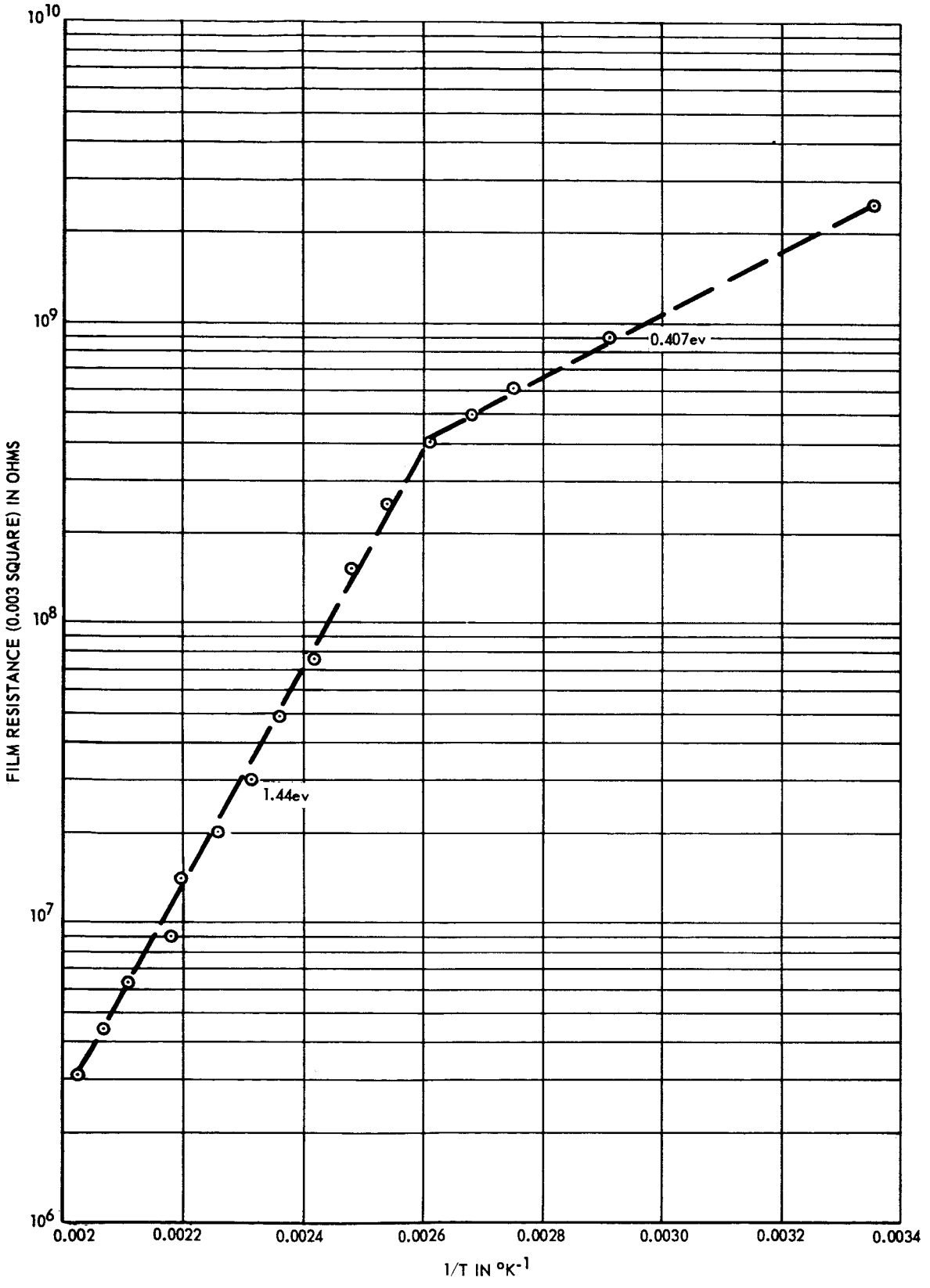

Figure 8. Resistance vs. 1/T for CdTe Thin Film

The CdTe films were prepared in a dual bell jar vacuum system (see 2nd Quarterly Report, p. 20) by evaporation of high-purity CdTe (Penn Rare Metals) from a graphite crucible heated to 800°C. Vacua of 5×10^{-7} torr could be attained before the start of the CdTe evaporation and held to less than 6×10^{-6} during the evaporation. The films were deposited on 1 x 1 in., 20-mil, Corning 0211 glass substrates with vacuum-deposited nichrome contacts (.003 square between contacts). The substrates were heated to 400°C and cooled to 90°C in vacuum immediately before the CdTe evaporation. The films were then heated in vacuum to 300°C for 2 minutes and either cooled in vacuum or immediately quenched in air. Film thicknesses ranged between 2500 Å and 7500 Å and the film resistances were always greater than 10^9 ohms (.005 squares), except for films deposited from the first evaporation of a newly loaded crucible of CdTe. It was observed that there was a small percentage of excess Cd or Te in the new material which evaporated at a lower temperature than the compound. Films formed on the first run of new material had resistances ranging from 1 ohm to 100 megohms, depending upon how much of the compound was also evaporated. Upon annealing these films in vacuum, their room-temperature resistance rose steadily to greater than 10^9 ohm. It is believed that the anneal merely selectively evaporates the excess constituent and forms a more stoichiometric film.

TFTs were formed from the various CdTe films described above by evaporation of a 1500 Å SiO film as the dielectric and a 500 Å Al film as the gate electrode. The general results were as follows:

(a) No field effect was detected, either on low-resistance films or on high-resistance films which had been cooled in vacuum after the vacuum anneal.

(b) n-type field effect was observed on high-resistance films which had been quenched in air following the vacuum anneal. Transconductances of 10 micro mhos were reached.

(c) The deposition of SiO did not appreciably change the film resistance on any of the films.

2.4.2 Cadmium Telluride Doped with Indium

The curve of log of resistance versus reciprocal of absolute temperature for a CdTe film doped with indium is shown in figure 9. The film resistance is reversible over the range from 25° to 250°C. At temperatures below 70°C, the slope of the curve indicates an ionization energy of 0.0234 ev. This is in good agreement with the reported values summarized by Glang[4] of 0.02 ev.

The indium-doped CdTe films were prepared by coevaporation of the two materials from separate boats. A graphite crucible heated to 800°C was used for the CdTe and a 20-mil tungsten boat heated to 900° C was used for the indium. The films were deposited on the same type of substrates used previously for undoped CdTe. The substrates were similarly heated and cooled in vacuum immediately before the film deposition. Following the film deposition, the films were either annealed in vacuum and quenched in air, or merely baked in air. Film thicknesses ranged between 1600 Å and 5000 Å. The film resistances were generally high (10^6 to 10^9 ohms) before any heat treatment. During the anneal cycle, either in vacuum or air, the film resistance initially increased to 10^8 ohms or greater and then dropped rapidly by three to five orders of magnitude to form a highly n-type film. The initial increase in

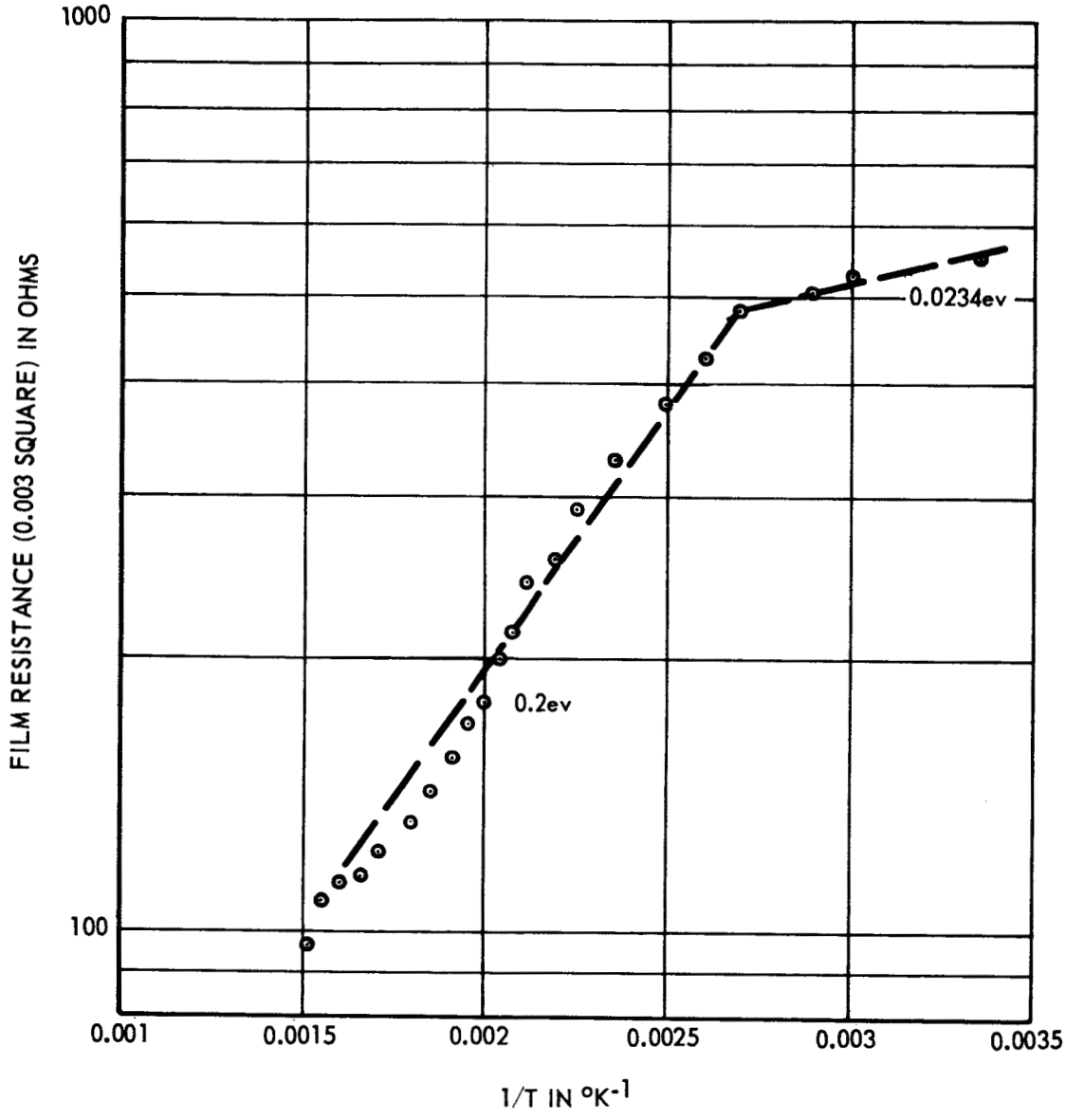

Figure 9. Resistance vs. 1/T for CdTe Thin Film Doped with Indium

resistance is probably due to the introduction of acceptor trapping levels in the CdTe by oxygen, which is a p-type dopant for CdTe.[5] The large drop in resistance with increased heating is the result of the diffusion and incorporation of the indium within the CdTe.

SiO deposited onto the films caused an additional decrease in resistance by two to three orders of magnitude. The films used in the fabrication of TFTs were baked in air just long enough for the film resistance to pass through the initial increase in resistance. The application of SiO then reduced the film resistance by two to four orders of magnitude and yielded a usable film resistance. The field effect observed was n-type, perhaps indicating that the SiO is "gettering" oxygen from the films surface and forming an n-type layer at the dielectric-semiconductor interface. Figure 10 shows the output characteristics of a CdTe:In TFT with a transconductance of 500 μ mhos. TFTs made with films which had been heated until their resistance dropped by three to five orders of magnitude generally had smaller transconductances and the output current could not be biased completely off.

2.4.3, Cadmium Telluride Doped with Iodine

CdTe films doped with iodine were formed, and TFTs using these films were fabricated. Figure 11 shows the log of resistance versus the reciprocal of absolute temperature for a heavily doped low-resistance film. The slope of the curve indicates ionization energies of 0.128 ev from 25° to 175°C and 0.058 ev from 175° to 230°C. The resistance of the film was completely reversible within this temperature range. The calculated

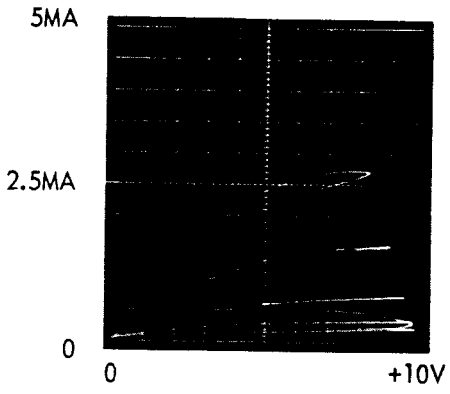

V_g = 2V/STEP
R_L = 1K OHM
BIAS = -1.6V
n-TYPE MODULATION

Figure 10. Output Characteristics of CdTe Doped with Indium TFT

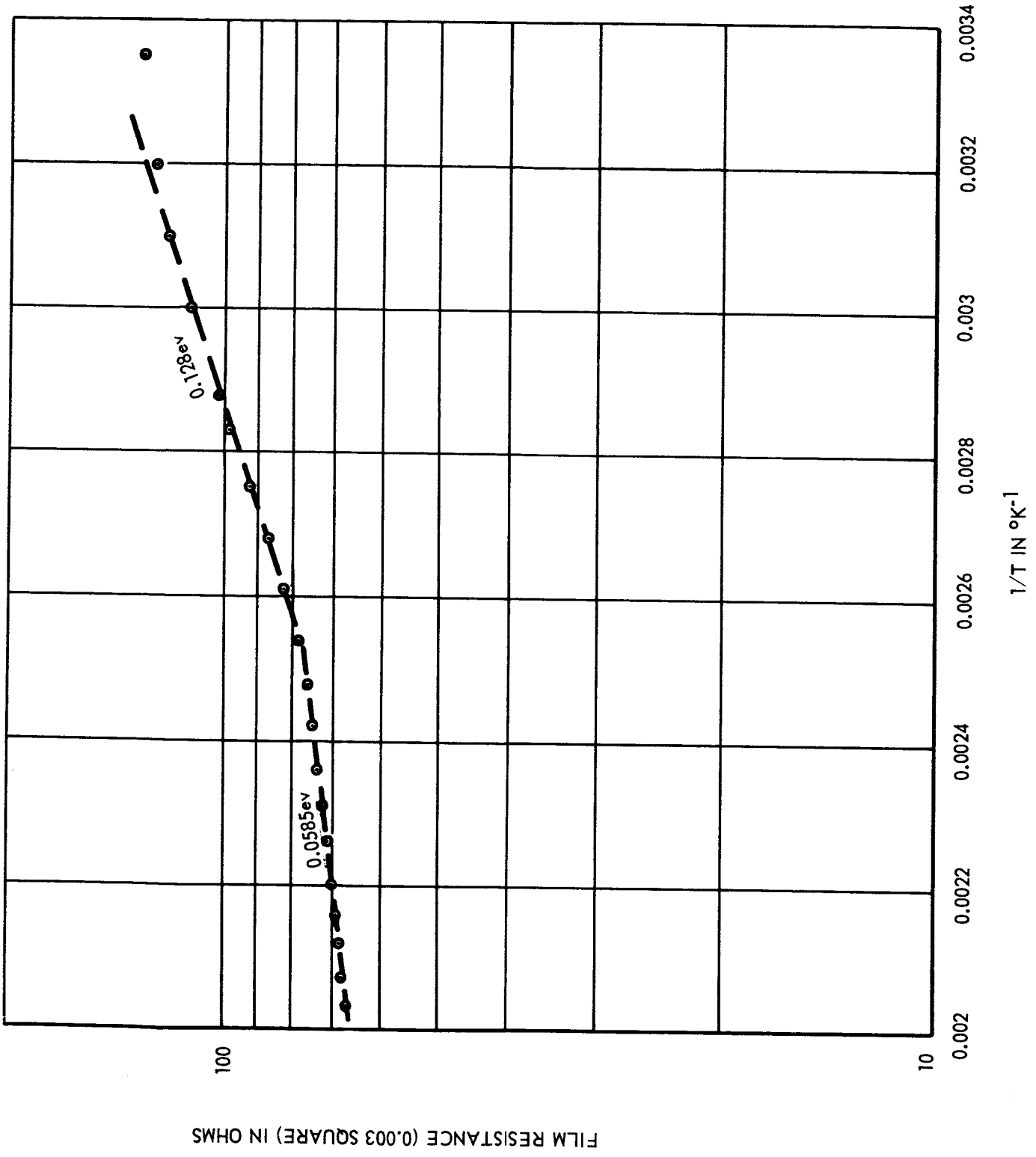

Figure 11. Resistance vs. 1/T for CdTe Doped with Iodine

ionization energies do not agree with the accepted ionization energies for iodine reported by Bube[3] and others of 0.003 to .01 ev.

It is believed that the iodine impurity levels are completely ionized at room temperature and, thus, would not play a dominant role in the conduction mechanism over the temperature range shown in figure 11.

The deposition procedures for CdTe:I films were the same as those for the CdTe:In films, except that the substrate temperature was 25°C and the films were given no heat treatment following the deposition. Vacua of 5×10^{-6} torr could be attained before the start of the coevaporation and held to less than 5×10^{-4} during the deposition. The increase in pressure is due to the extremely high vapor pressure of iodine. Film thicknesses ranged from 2500 Å to 1 μ, and film resistances generally varied from 10^6 to 10^9 ohms. The evaporation of SiO onto the CdTe:I films caused a large decrease in film resistance by three to four orders of magnitude. This large decrease in resistance is believed to be due mainly to the heating of the CdTe:I film during the SiO deposition and subsequent iodine diffusion, not to the "gettering" action of the SiO. No field effect was detected on completed TFTs.

2.5 High-frequency Measurement Technique

During the past report interval, a test procedure has been developed to evaluate the frequency response of the active devices for future circuit applications. Two parameters have been measured. The first is the gain-bandwidth product; the second is the maximum frequency of oscillation. The gain-bandwidth product is a measure of the limitations imposed by the device

capacitance, while the maximum frequency of oscillation is limited only by the mobility or transit time of the charged carriers.

A circuit diagram is shown in figure 12 for the measurement of gain-bandwidth product. A variable-frequency, constant-voltage signal generator supplies the signal to the device under test. A 10K ohm resistor load is used to develop the amplified signal. As the frequency of the applied signal is increased, the output voltage is monitored. When the output falls to half power, the frequency is recorded. The product of the low-frequency gain and the half-power frequency is the gain bandwidth in cps. The capacitance is about equal to the device input capacitance, so that the measurements are approximately the same as would be encountered when the devices are used in a multistage amplifier.

For higher-frequency work, it is normal to use inductors to reasonate with the device and circuit capacitance. When this is done, the device is able to maintain the gainbandwidth product at frequencies up to the point where the device is limited by transit-time effects. For this reason, a test procedure has been developed to check the maximum frequency of oscillation. This circuit is shown in figure 13. The circuit is a Colpitts oscillator and lends itself to inductive tuning. With the use of high-Q coils, the maximum frequency of oscillation is determined by the active device under test.

The thin-film devices tested to date have a gain-bandwidth product of about 10 mcs, with a maximum frequency of oscillation of about 20 mcs. Actually, if the gain-bandwidth is computed without the load capacitance

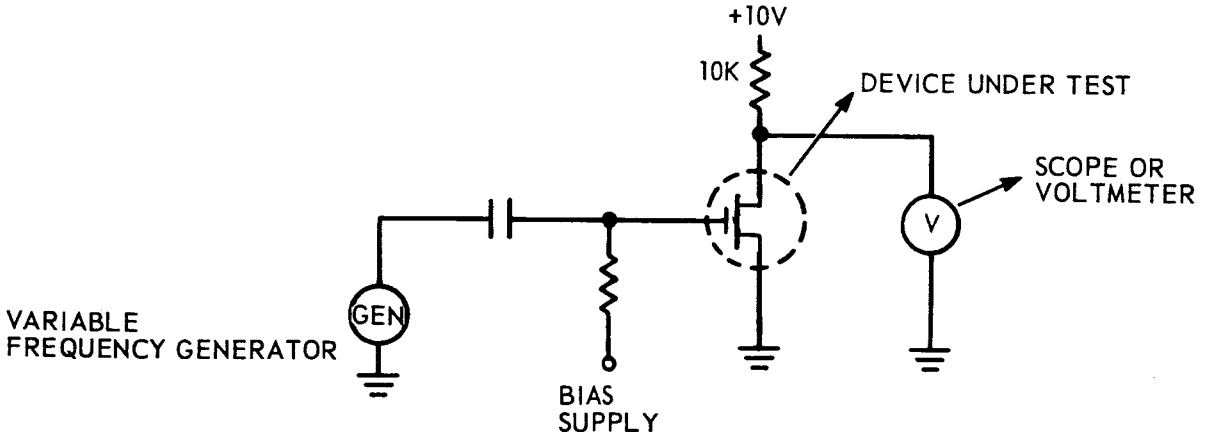

Figure 12. Gain-bandwidth Product Measurement Circuit

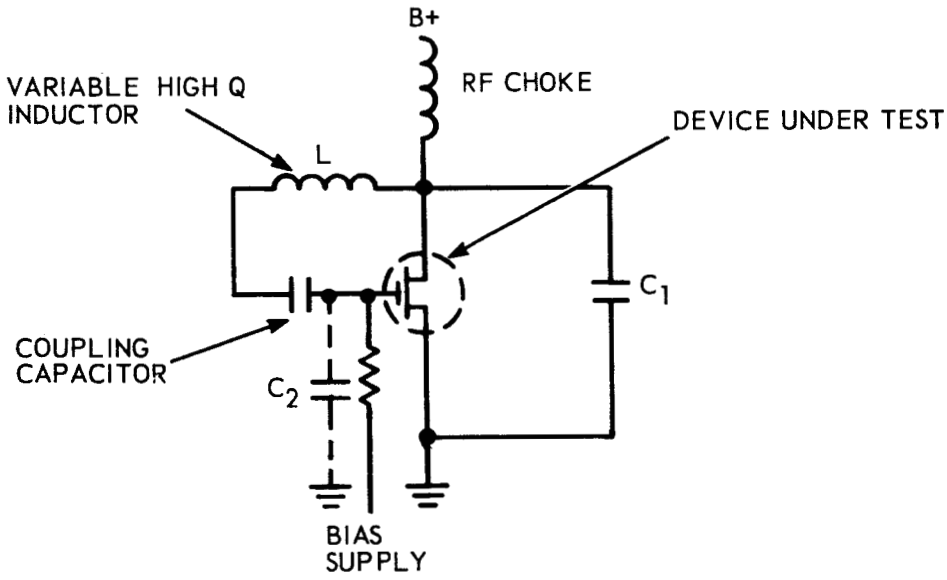

Figure 13. Maximum Frequency of Oscillation Measurement Circuit

(of the measuring instrument), it is about 20 mcs. The frequency response in both cases is then limited by the mobility of the semiconductor. However, from a practical standpoint, the first-mentioned figures are the usable values.

A typical thin-film device used for these tests was a CdSe TFT with a source-drain spacing of 0.2 mils, a length of 25 mils, and a gate 1 mil wide. A Te TFT with the same dimensions, except that the source-drain was 100 mils long, demonstrated approximately the same performance characteristics. The Te device was capable of operation in excess of 100 milliwatts.

The tests will be repeated with narrower gates, as discussed in section 2.1.

3. METAL-BASE TRANSISTOR AND DIODES

The materials-evaluation phase of the metal-base transistor work was continued throughout most of the third quarter. The primary reason for extending this phase of the work was the lack of supply of ZnSe from Penn Rare Metals, Inc. As reported in the second quarterly, this material was compatible with CdSe from Koch-Light for forming transistor-quality junctions. The ZnSe materials from the other suppliers formed junctions with relatively low reverse breakdown voltages. Penn Rare Metals, Inc., however, no longer supplies electronic-grade ZnSe. Therefore, it was necessary to find another supplier.

Junctions formed from the ZnSe supplied by Koch-Light Laboratories, Ltd., exhibited characteristics comparable to the junctions formed from the ZnSe supplied by Penn Rare Metals, Inc. The search for a ZnSe supplier will, therefore, be terminated and a major portion of the effort will be directed toward the study and improvement of the junctions formed from the CdSe and ZnSe supplied by Koch-Light Laboratories, Ltd. Work on the "reverse" junction has just been initiated. The main effort will now be directed toward fabricating the "reverse" junction and the completion of a metal-base transistor structure.

3.1 Summary of Results of ZnSe Materials Evaluation

Figure 14 shows the I-V characteristics of a junction formed by depositing a mixture of ZnSe and CdSe supplied by Koch-Light Laboratories, Ltd. Its characteristics are given in table I, along with the characteristics of the junctions formed from ZnSe from the different suppliers. For

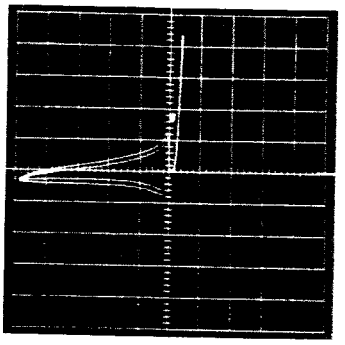

SCALE:

FORWARD BIAS 0.2 MA DIV - VERTICAL
2V DIV - HORIZONTAL

REVERSE BIAS 0.01 MA DIV - VERTICAL
2V DIV - HORIZONTAL

Figure 14. Characteristics of CdSe-ZnSe Thin-film Junction Using CdSe and ZnSe from Koch-Light Laboratories Ltd.

Table I

CHARACTERISTICS OF JUNCTIONS FORMED FROM ZnSe FROM DIFFERENT SUPPLIERS

(Junction area = 5.81×10^{-2} cm^2)

ZnSe supplier	Peak inverse voltage (volts)	Forward breakdown voltage (volts)	Rectification ratio	Forward resistance (ohms)	Leakage Current at -4 volts (μa)
Penn Rare Metals, Inc.	8-10	0.3-0.8	10^4-10^5 at 1 volt	$\lesssim$ 100	$\lesssim$ 1
Koch-Light Laboratories, Inc.	8-10	0.2-0.6	10^4-10^5 at 1 volt	$\lesssim$ 100	$\lesssim$ 1
Metal Hydrides, Inc.	5-6	2-3	10^4 at 3 volts	$\lesssim$ 500	$\lesssim$ 1
Harshaw Chemical Co.	3-4.5	0.4-0.8	10^4 at 1 volt	$\lesssim$ 500	$\lesssim$ 2
Kern Chemical Corp. (Luminescent grade)	6	0.3-0.8	10^4-10^5 at 1 volt	$\lesssim$ 200	$\lesssim$ 1
Eastman Kodak Co.	3-4	0.3-1.5	10^4 at 1 volt	$\lesssim$ 500	$\lesssim$ 3
Kawecki Chemical Co. (Luminescent grade)	3-4	0.3-1.5	10^4 at 1 volt	$\lesssim$ 500	$\lesssim$ 3

completeness, the results of the spectrographic analysis report on the different ZnSe materials and on the CdSe from Koch-Light are shown in table II.

3.2 Capacitance-Voltage Measurements

The presence of a Schottky-type barrier at the "blocking" contact was established by means of differential capacitance measurements. Figure 15 presents these measurements in a plot of $1/C^2$ vs. V. From the slope of $1/C^2$ vs. V, one is able to determine the space-charge density profile as well as the barrier height between the gold electrode and the ZnSe-enriched boundary of the semiconductor film. The change in slope in the plot shown in figure 15 indicates a change in the space-charge density from $N_1 \simeq 5.7 \times 10^{14}$ cm^{-3} to $N_2 \simeq 4.2 \times 10^{16}$ cm^{-3}. The intercept of the $1/C^2$ vs. V plot with the V axis gives a barrier height of 0.45 ev.

3.3 Switching Characteristics

The Tektronix, type S, unit, a special-purpose plug-in unit, was used to display the junction-switching characteristics. The display shows the voltage across the test junction as a function of time during the desired switching operation. Certain diode parameters, such as the effective lifetime of minority carriers, junction capacitance, stored charge at the junction, and junction resistance, can be readily obtained from the display.

3.3.1 Forward Recovery Time

Typical junctions, 5.81×10^{-2} cm^2 in area, exhibited forward recovery times of 0.5 μsec, 0.3 μsec, and 0.1 μsec when switched from the "off" state (-2.5V) to forward currents of 1 ma, 2 ma, and 5 ma respectively. The

Table II

SPECTROGRAPHIC ANALYSIS REPORT OF
MATERIALS FROM VARIOUS SUPPLIERS

Material	Supplier	Impurities	Faint Impurities (<< 0.001%)	
ZnSe	Penn Rare Metals, Inc.	Ca (~0.001%) Pb (~0.01%) Mg (~0.001%)	Al Cu Fe	Si Sr
ZnSe	Koch-Light Laboratories, Inc.	B (~0.001%)	Cu Mg Sr	
ZnSe	Matal Hydrides, Inc.	Fe (~0.005%) Cu (< .001%) B (~0.01%) Ca (~0.001%)	Al Cu Mg	Mn Si Sr
ZnSe	Harshaw Chemical Co.		Al Cu Fe	Mg Si Sr
ZnSe	Kern-Chemical Corporation	Ca (~.001%) Cu (~0.005%) Al (~0.005%)	Fe Si Sr	
ZnSe	Eastman Kodak Co.		Al Cu Fe	Si Sr Ti
ZnSe	Kawecki Chemical Co.	B (~0.001%) Pb (~0.001%)	Mg Si Sr	
CdSe	Koch-Light Laboratories, Inc.		Cu Mg Zn	

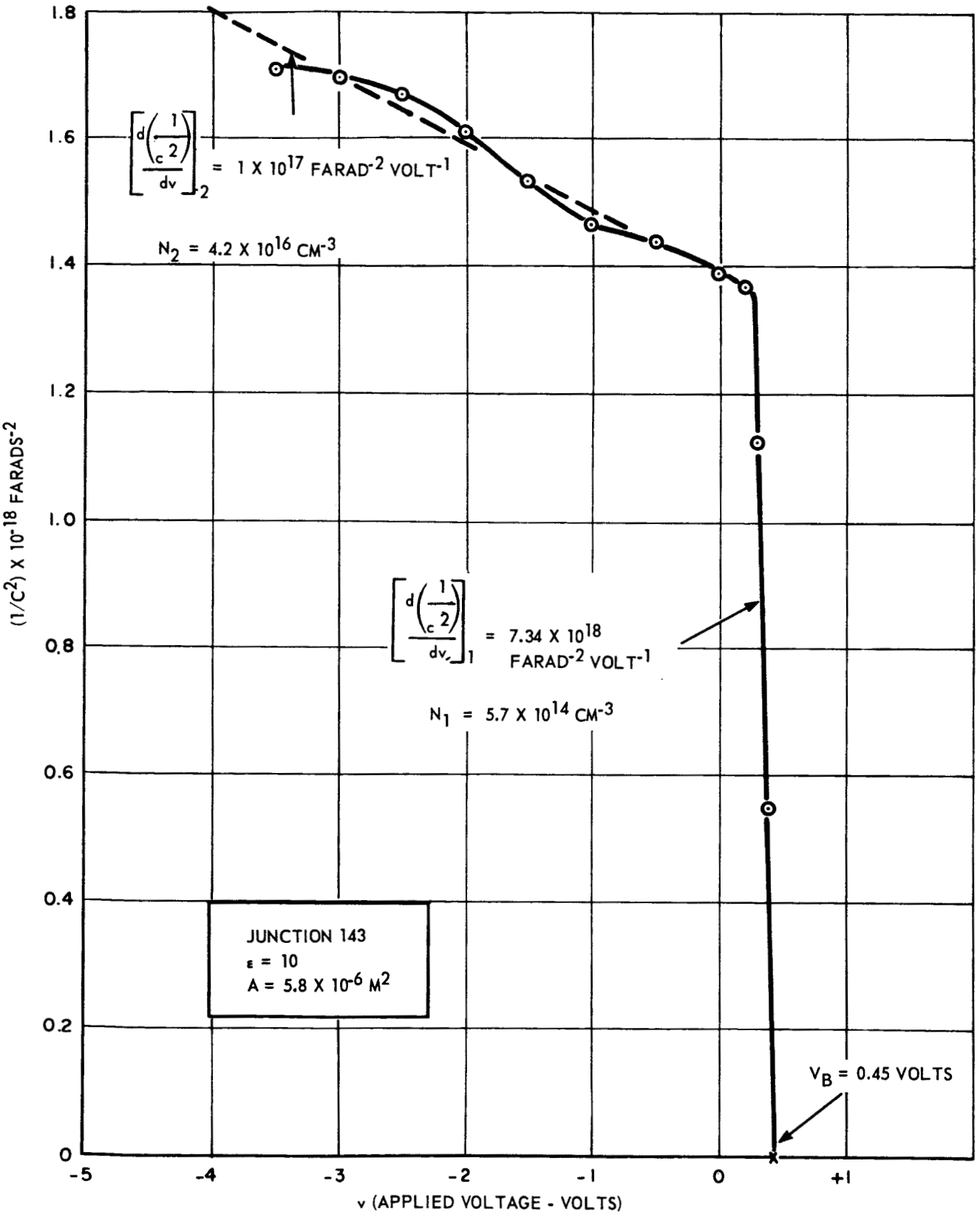

Figure 15. Differential-capacitance Measurements

forward recovery time is defined as the time required for the voltage across the junction to reach its steady-state value after the forward switching pulse is applied. The interesting observation made in the "turn-on" characteristics is the absence of a switching transient normally observed in p-n junctions. This switching transient is an initially high forward impedance caused by the redistribution of minority carriers in the semiconductor materials. The absence of this transient indicates the insignificance of the minority carrier conduction in CdSe-ZnSe junction.

3.3.2 Reverse Recovery Time

The reverse recovery time, defined here as the time required for all excess minority carriers to either be recombined or withdrawn from the semiconductor material, can be measured by observing the reverse switching characteristics of the junction. Since this time is a function of the recombination rate of minority carriers, the amount of stored charge and the reverse current, the junctions were switched off from forward currents of 1 ma, 2 ma, and 3 ma to reverse currents of 0.1 ma, 0.2 ma, and 0.5 ma. In all cases, the reverse recovery time was measured as zero, indicating the absence of minority carriers. The only delay in switching was caused by the charging time of the junction capacitance. Typical charging times for junctions (5.81×10^{-2} cm^2 in area), when switched from a forward current of 1 ma to reverse currents of 0.1 ma, 0.2 ma, and 0.5 ma, were 30 μsec, 15 μsec, and 6 μsec respectively. These times were found to be almost independent of the forward current before switching. This is as expected since there is no charge storage.

3.3.3 Comparison with p-n Junction

The conclusion from these measurements is that these CdSe-ZnSe junctions should be faster than conventional p-n junctions by an amount given by the reverse recovery time. This is, of course, assuming similar values of equivalent series resistance and capacitance for the junctions.

To verify this, the switching characteristics of a smaller-area CdSe-ZnSe junction were compared to those of a 1N138A germanium diode. The CdSe-ZnSe junction exhibited the following characteristics: Forward recovery time (when switched from -2.5 V to 1 ma) = 0.04 μsec; reverse recovery time (when switched from 1 ma to 0.1 ma) = 0; total reverse switching time (when switched from 1 ma to 0.1 ma) = 1.8 μsec. The 1N138A germanium diode exhibited the following characteristics when switched from the same values of forward and reverse currents and voltages as the CdSe-ZnSe junction: Forward recovery time = 0.03 μsec; reverse recovery time = 0.7 μsec; total reverse switching time = 1.8 μsec.

The equivalent series resistance and capacitance, measured at 100 Kcps and zero bias, for the CdSe-ZnSe junction was 2.23 KΩ and 116.3 pf, respectively. The values for the 1N138A diode, measured under the same conditions, were 396 Ω and 20.8 pf. From this, one would expect the CdSe-ZnSe junction to be about 30 times slower than the 1N138A diode. A comparison of the forward recovery times and the total reverse recovery times, however, shows the junctions to be of equal speed. Hence, for similar values of series equivalent resistance and capacitance, the CdSe-ZnSe junction can be expected to be faster.

The frequency response of the CdSe-ZnSe junctions is, therefore, limited only by the charging time of the junction capacitance since junction currents involve one-carrier transport.

3.4 Varactor Diodes

Since the mechanism of operation of the Au-CdSe/ZnSe-Au diode is based upon a voltage-sensitive space-charge layer, its varactor characteristics merit investigation.

The varactor operation of such a device is not generally familiar, and the theory of operation is, therefore, briefly outlined here. An n-type semiconductor with a fully ionized, uniform donor density is assumed to be in contact with a metallic layer. Integration of Poisson's equation throughout the depletion region yields a solution which relates the depletion layer thickness, x, to the applied voltage, V_a. The solution can be written as

$$x = \left[\frac{2\epsilon\epsilon_o \ (V_B - V_a)}{q \ N_D} \right]^{1/2} \tag{1}$$

where ϵ is the relative dielectric constant of the semiconductor, ϵ_o is the permittivity of free space, V_B is the barrier height at the metal semiconductor contact, q is the electronic charge, and N_D is the donor density. The junction capacity can be expressed as

$$C = \frac{dQ}{d(V_B - V_a)} \tag{2}$$

where Q is the total space-charge. Q can, thus, be written as

$$Q = A \ qN_D x \tag{3}$$

where A is the junction area. Combining equations (1), (2), and (3) and carrying out the differentiation of eq. (2) yields

$$C = A \left[\frac{\epsilon\epsilon_o q N_D}{2(V_B - V_a)} \right]^{1/2} \tag{4}$$

Equation (4) represents the varactor operation of the metal semiconductor junction. The capacitance is seen to decrease under negative bias and increase with positive bias. It is noted that the plot shown in figure 15 is in agreement with eq. (4).

The capacitance ratio is

$$\frac{C_{max}}{C_{min}} = \frac{V_B - V_{piv}}{V_B} \tag{5}$$

where C_{max} is defined here as the zero bias capacitance and C_{min} is the capacitance at maximum reverse-bias voltage, V_{piv}. If one assumes V_{piv} = 3.5 volts and V_B = 0.45 volts, he would expect a capacitance ratio of 2.78. The junction characteristics plotted in figure 15 indicate a V_B of 0.45 volts. Taking the reverse bias voltage at 3.5 volts yields a capacitance ratio of only 1.11. This discrepancy between theory and experiment is attributed to the nonuniformity of the effective space-charge density in the depletion region.

Due to the finite series resistance of the semiconductor, there is a cut-off frequency given by

$$F_{co} = Q\,F = \frac{1}{2\pi RC} \tag{6}$$

where Q is the quality factor of the junction and F is the measurement frequency. R and C are the effective-series resistance and capacitance of the junction.

The cut-off frequency at zero bias can be expressed in terms of the semiconductor-material properties. The junction series resistance can be written as

$$R = \frac{L}{q\mu N_D A} \tag{7}$$

where L is the semiconductor thickness and μ is its effective carrier mobility. It is assumed here that $L \gg x_o$, where x_o is the zero bias depletion region thickness. The zero bias cut-off frequency can, thus, be written as

$$F_{co}\ (\text{o bias}) = \frac{\mu}{2\pi L}\left[\frac{2qN_D V_B}{\epsilon\,\epsilon_o}\right]^{1/2}. \tag{8}$$

Equation (8) shows that a large value of μ, N_D, and V_B, and a small value of L, are desired for high cut-off frequency. It is noted, however, that increases in V_B and/or N_D reduce the capacitance ratio. Hence, there is an optimum set of material parameters.

Preliminary varactor measurements were performed on units with 7500 Å-thick semiconductor and 5.81×10^{-2} cm^2 area. Measurements were made with a capacitance bridge using a 1/2-volt, 100-kc signal. Typical values for the capacitance ratio, obtained over a bias range of 3.5 volts, ranged from 1.1 to 1.2. The relatively large area restricted the zero bias cut-off frequency of these units to about 1.5 mc. With a reduction in junction area, it is possible to increase the cut-off frequency by several orders of magnitude.

4. INDUCTORS

In the first quarterly report, the theory of the various facets and phenomena pertinent to thin-film inductors was discussed. The equations required for the calculation were presented. Various multiturn thin-film coils were evaluated. In the second quarterly report, the equations were tabulated and the theory of inductors, as applied to thin films, further evaulated in the light of experimental and practical uses. As discussed, the most apparently useful inductors would be of low inductance values. The resulting shorter coil length would provide higher self-resonant frequencies, better Q values due to lower resistance, and would provide coils with sufficient inductance to be useful at lower frequencies, including use in tank circuits, since the capacitors would have high enough values for precision trimming.

4.1 High-frequency Inductors

Table III lists the inductors formed during this quarter. They are all one-turn coils (as shown in figure 16), with the outer diameter and conductor widths varied for comparison.

4.2 Deposition Parameters

Chromium was deposited first for better substrate adhesion, and copper was deposited to a mean thickness of approximately 2.9 microns. The copper thickness varied across the substrate pallet plus or minus 10 percent. Since substrate Y1 has the most squares, it yields the most accurate value of ohms per square. The ohms per square are 0.00536 for a coil (Y1) with 104 squares and a copper thickness of 30,750 angstroms. This value of ohms

Table III

HIGH-FREQUENCY INDUCTORS

Substrate	Outer Diameter (inches)	Width (inches)	Length (inches)	R_{dc} (ohms)	R_{ac} (ohms) 200 mcs	L(μh) 200 mcs	Q 200 mcs	Theoretical f_o(mcs)
Y 1	0.8	0.025	2.6	0.557	1.864	0.0680	45.8	570
Y 2	0.8	0.050	2.6	0.306	1.714	0.0553	40.7	570
Y 3	0.8	0.100	2.35	0.123	0.882	0.0461	65.8	630
Y 4	0.8	0.150	2.15	0.062	0.625	0.397	79.9	689
Y 5	0.6	0.025	1.8	0.395	1.524	0.0534	44	823
Y 6	0.6	0.050	1.8	0.189	0.972	0.0420	54.3	823
Y 7	0.6	0.100	1.65	0.080	0.668	0.0383	72.1	897
Y 2A	0.8	0.050	2.6	0.273	1.25	0.538	54	570
Y 6A	0.6	0.050	1.8	0.181	1.366	0.0459	42.2	823
Y 8	0.4	0.050	1.1	0.115	0.915	0.396	54.4	1345
Y 9	0.5	0.050	1.5	0.116	1.1	0.0452	51.6	988
Y 10	0.5	0.100	1.25	0.065	0.644	0.368	72	1182

Note: Substrates are Corning, code 0211, glass.

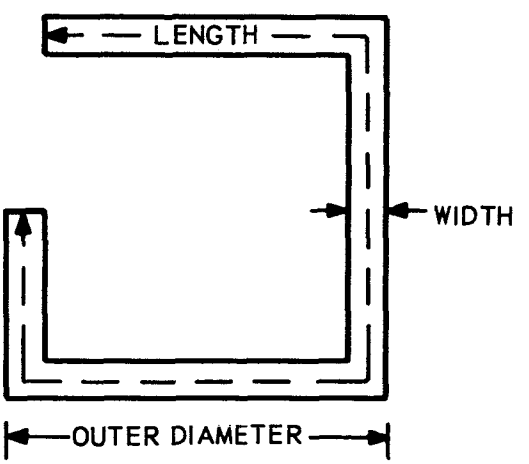

Figure 16. One-turn High-frequency Inductor

per square at this thickness calculates to within the experimental error for the bulk resistivity of copper (1.7241×10^{-6} ohms•cms), as discussed in the second quarterly report.

4.3 Experimental Results

In table III, the inductors are grouped. Substrates Y1 through Y4 all have the same outer diameter, 0.8 inches, but the conductor width has been varied. Substrates Y5 through Y7 have the same outer diameter, 0.6 inches, and the conductor widths have also been varied. The changes in resistance as a function of frequency for these two sets have been plotted in figures 17 and 18. This change is, of course, due to the skin effect on the conductors. The skin depth of copper at 100 mcs is 66,100 angstroms, and at 250 mcs is 41,800 angstroms. Figures 19 and 20 show the same coil groups with the inductance plotted as a function of frequency. The reason the inductance increases with frequency can be most basically explained by examining the equation for voltage (v) across an inductor (L) with a changing current (i) applied.

$$v = L \frac{di}{dt}$$

However, since the resistance is changing due to the skin effect, the current is, therefore, also changing as a function of frequency. The basic definition of inductance (L) is the flux linkage divided by the current.

$$L = \frac{N\Phi}{i} \quad \text{(weber•turn per ampere)}$$

Therefore, since the current is changing, the inductance is changing and the voltage across the inductor is actually a function of the inductance and the current, which is what the Q meter correctly reads.

$$v = \frac{d(Li)}{dt}$$

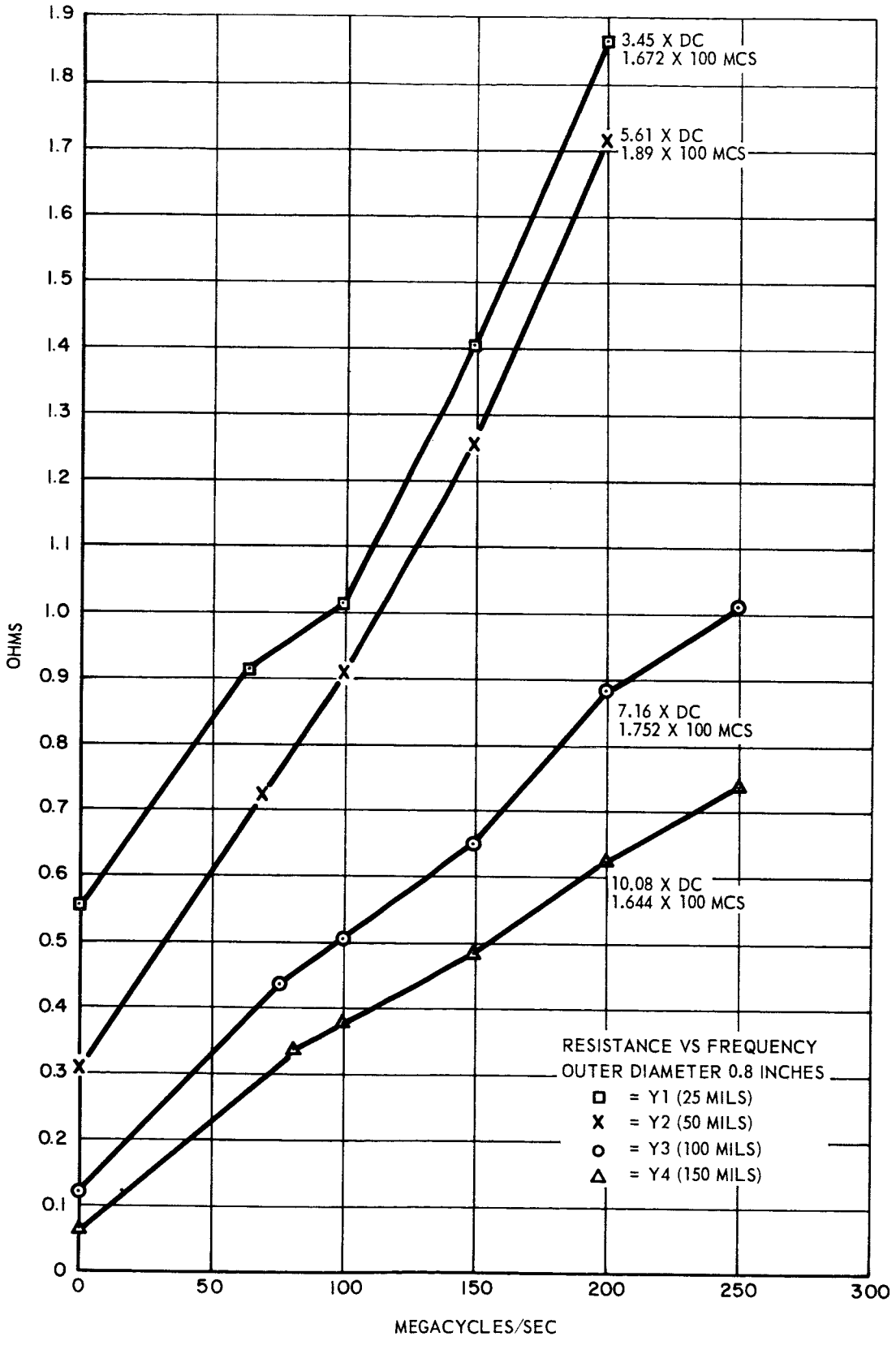

Figure 17. Resistance vs. Frequency, Outer Diameter 0.8 Inches

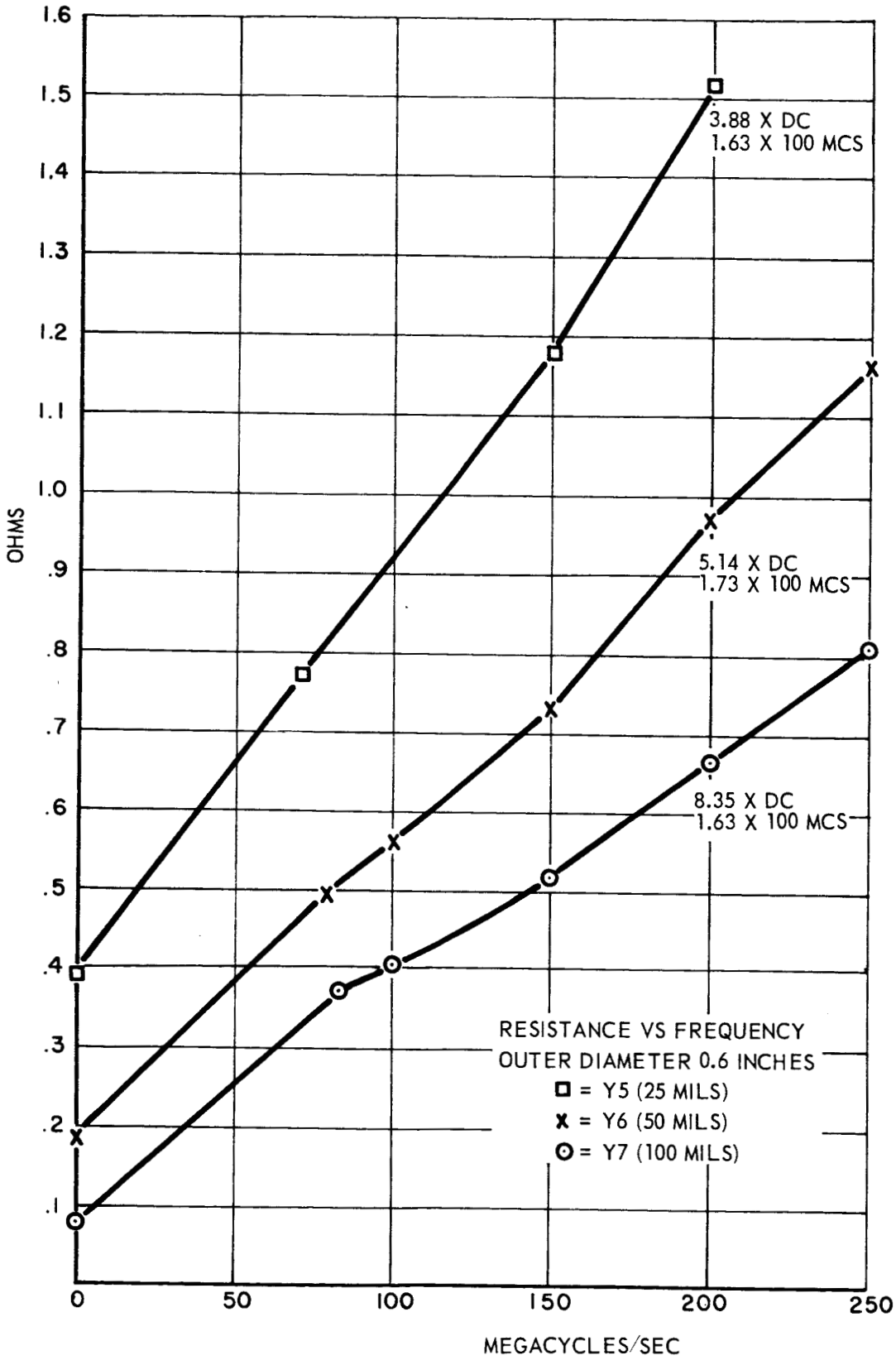

Figure 18. Resistance vs. Frequency, Outer Diameter 0.6 Inches

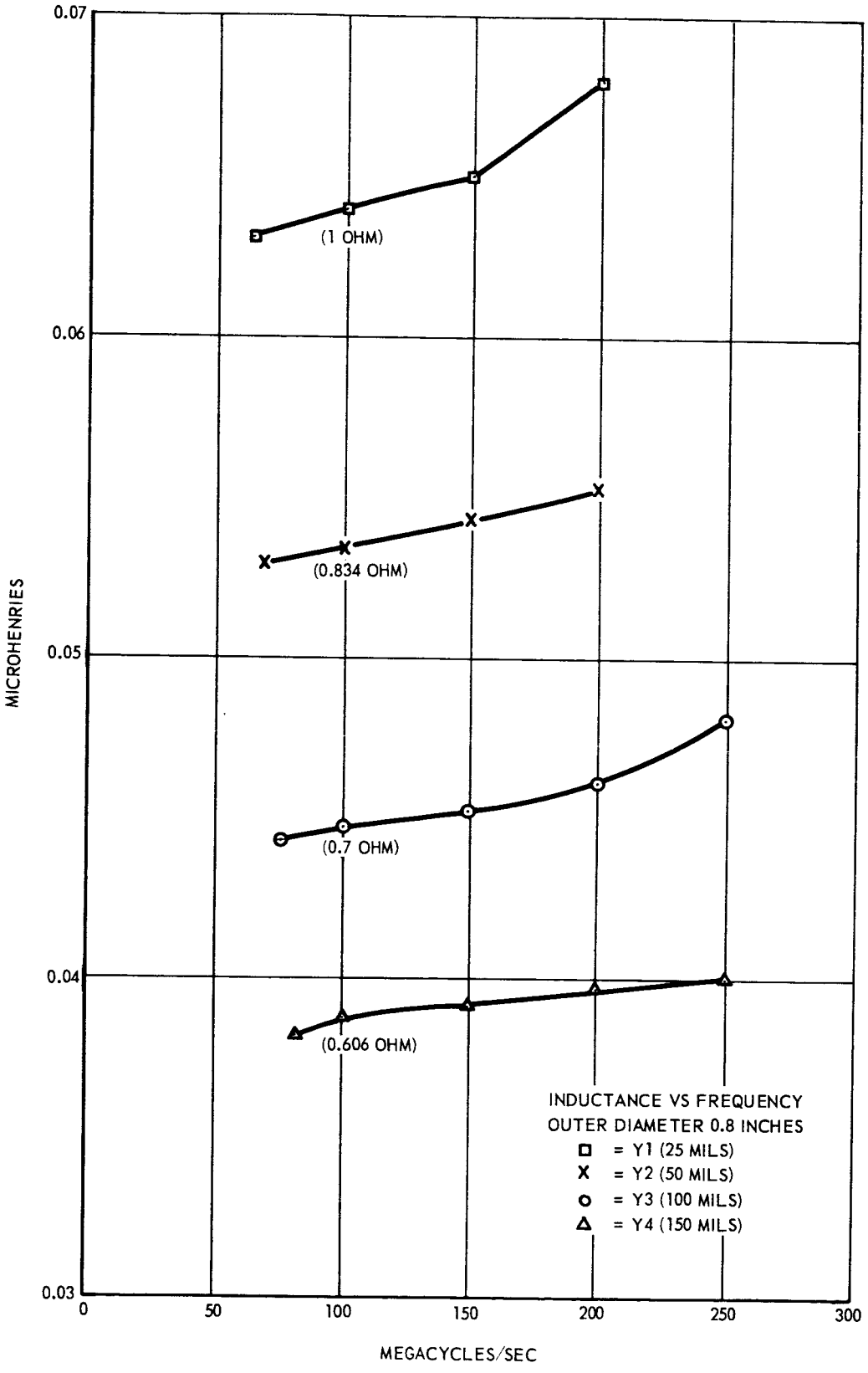

Figure 19. Inductance vs. Frequency, Outer Diameter 0.8 Inches

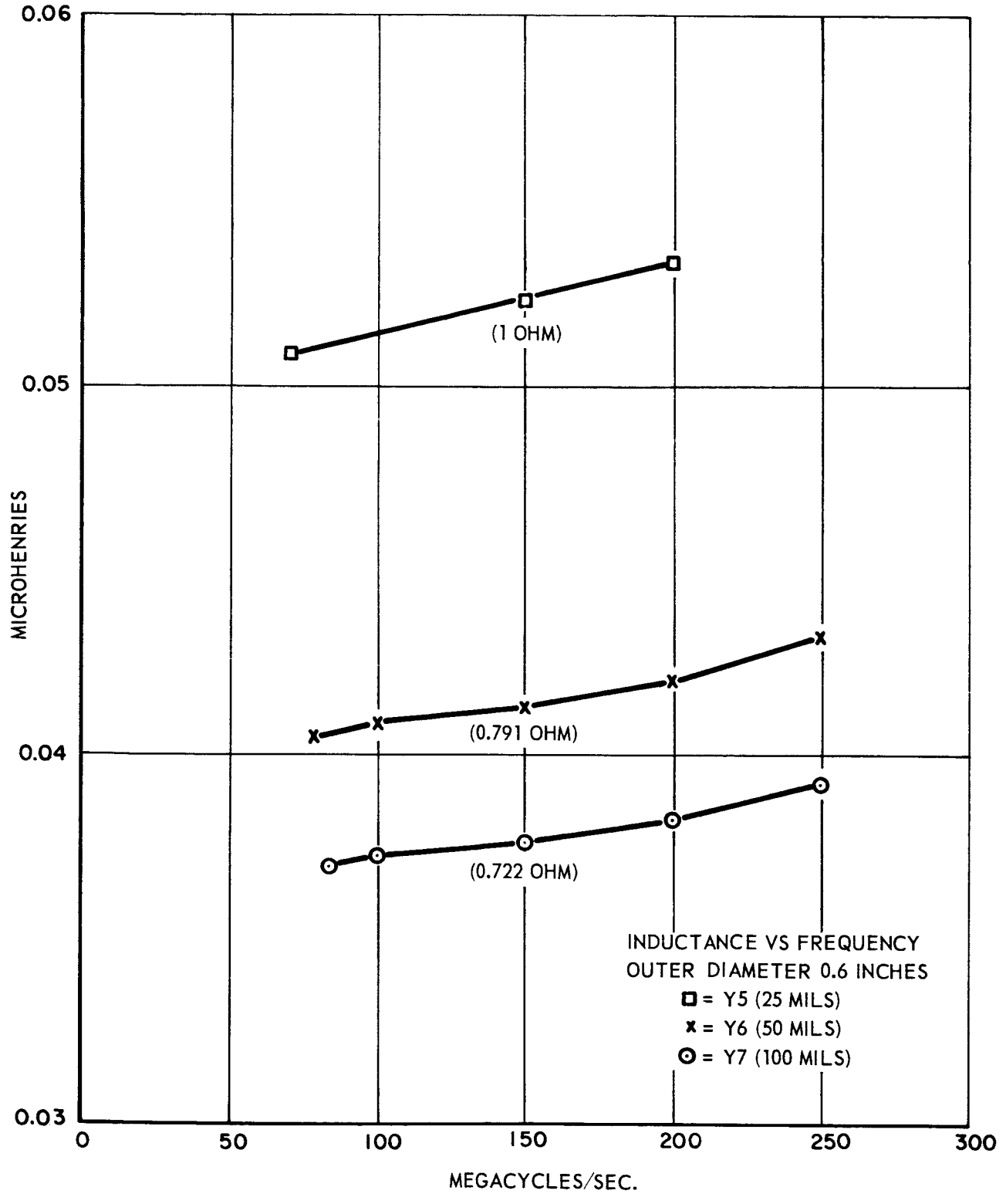

Figure 20. Inductance vs. Frequency, Outer Diameter 0.6 Inches

All the plotted values are shown in table IV. The self-resonant frequency of these coils is undetermined. The Q meter (Boonton Radio Corp., 190-A) will not go high enough in frequency to even approach the self-resonance of these coils. The theory for self-resonance (second quarterly report) should hold true for this configuration coil and result in theoretical self-resonant frequencies ranging from 570 mcs to 1345 mcs, which are well beyond the requirements of this program. Also, it should be noted that the Q meter does not give accurate results when the resonating capacitor is used below 10 picofarads. That is the reason that some of the coils in table IV do not have values shown for 250 mcs. For example, Y1 resonates with a 10-picofarad capacitor at just about 200 mcs.

Substrates Y2A and Y6A are the same as Y2 and Y6, except that squares of copper were deposited in the center of the coil. Y2A has a 0.3-inch square and Y6A has a 0.2-inch square. Any slight difference between Y2 and Y2A and Y6 and Y6A can be explained by experimental error and the plus or minus 10-percent variation in copper thickness. Therefore, the squares of copper in the center of the coils did not affect the coil values. Just how much of a mass (such as a transistor) could be placed there without degrading the performance would have to be determined.

Substrates Y8, Y9, and Y10 are presented for comparison of smaller outer-diameter coils.

4.4 Experimental Conclusions

Small-value inductors in thin-film form without any processing after vacuum deposition seem quite feasible. Inductances of 0.04 microhenries with a Q of 80 at 200 mcs are attainable on a one-inch substrate.

Table IV

INDUCTANCE AND RESISTANCE AS FUNCTION OF FREQUENCY

Substrate	Parameter	dc	Frequency (mcs) 100	150	200	250
Y 1	L (μh)		0.0640	0.0650	0.0680	
	R (ohms)	0.557	1.114	1.405	1.864	
Y 2	L		0.0534	0.0534	0.0553	
	R	0.306	0.907	1.254	1.714	
Y 3	L		0.0447	0.0452	0.0461	0.0481
	R	0.123	0.503	0.65	0.882	1.083
Y 4	L		0.0388	0.0392	0.0397	0.0405
	R	0.062	0.38	0.484	0.625	0.738
Y 5	L			0.0523	0.0534	
	R	1.183		1.183	1.524	
Y 6	L		0.0409	0.0413	0.0420	0.0433
	R	0.189	0.562	0.731	0.972	1.165
Y 7	L		0.0373	0.0377	0.0383	0.0392
	R	0.080	0.409	0.52	0.668	0.81

4.5 Circuit Considerations

These coils were formed by vacuum deposition only. By depositing for longer periods, the resistance could be decreased, resulting in higher Q values. Also, they could be electroplated or dip soldered to decrease the resistance.

When shielding is used, the inductor will be affected. The extent will be determined by the material used for shielding. Ferrite material would probably be best because any drop in Q would be offset by an increase in inductance. To roughly determine the effects of shielding, substrates Y1 and Y10 were connected to the Q meter with long, 5-mil gold wire leads and slipped into a can of copper foil. At 150 mcs, Y1 went from an L of 0.0784 microhenries and a Q of 48 to 0.0656 microhenries and a Q of 41.5 in the can. Y6 went from 0.0396 microhenries and a Q of 74.6 to 0.0362 microhenries and a Q of 64 in the can. These initial inductances are higher than stated in the tables due to the length of wire added to facilitate slipping the substrates in the cans. These changes would be constant after assembly of the hardware. It is necessary in any final design involving high frequencies to include the final packaging technique in the circuit design.

4.6 Inductor Program Conclusions

On one-inch substrates, coils have been formed to achieve different inductances. The largest inductance was achieved with series aiding multi-turn indicators on opposite sides of the substrate. In this manner, inductances up to 3 microhenries was achieved with a Q of 8 at 30 mcs and a self-resonant frequency of 54 mcs, as reported in the second quarterly report. On one side of a substrate, 1.5 microhenries with a potential Q of

15 at 30 mcs and a self-resonant frequency of 110 mcs can be deposited in 0.36 square inch, as reported in the first quarterly report. The emperical formulas for inductance and self-resonant frequency were used and modified for these multiturn inductors. These equations do not obviously fit the single-turn inductors reported here. No emperical formulas were developed since the need for these inductors has not been generated. If emperical formulas are necessary, they can be derived from the experimental results when the need for a particular value inductor is required. The single-turn inductors reported here do seem to be the most promising.

The results of the research into the effects of thin-film coils have been encouraging. Of course, the fact that thin-film coils are only two dimensional is a major limitation. However, since coils of this type are presently used (e.g., printed circuits), the potential exists for their use in vacuum-deposited monotronic circuitry.

4.7 Inductor Addendum

This addendum consists of corrections for the self-resonant frequencies given in the first and second quarterly reports. The previously-stated figures resulted from incorrect use of the Boonton Radio Corp. Q meter, 190-A. This instrument cannot be used accurately with its internal resonating capacitor set below 10 picofarads. When the scale is set at zero picofarads, there is a residual capacitance of approximately 7 picofarads in the equipment. A method was devised to obtain the self-resonant frequency through the use of the Boonton Radio Corp. RX meter, 250. The frequency is varied until the impedance is real (resistive only) without any external capacitance added to or substrated from the equipment's internal balancing capacitor. This

method is tedious since the test equipment must be rebalanced at each frequency. The self-resonance of a coil can be found, however, as long as it does not exceed the limits of the equipment, 250 mcs.

It should be noted that all other inductor measurements given prior to this report, except the self-resonant frequency, are correct. The self-resonant frequencies given in the first two quarterly reports are actually the frequencies at which the coils resonate with a capacitor of approximately 7 picofarads. Table V, from the first quarterly report, and table VI, from the second quarterly report, are repeated here with the corrected values of self-resonant frequency (f_o) for clarity and completeness.

The corrected values for f_o are much higher than the previous values, which obviously increases the usefulness of these inductors.

Table V

(First Quarterly Report)

INDUCTOR VALUES

Substrate	Conductor width (mils)	Space (mils)	Outer diameter (inches)	Inner diameter (inches)
1	10	10	0.4	0
2	25	25	0.8	0
3	35	15	0.8	0
4	15	35	0.8	0
5	10	10	0.6	0

Substrate	Theoretical L(μh)	Theoretical f_o(mc)	Actual L(μh)	Actual f_o(mc)	Q (30 mc)
1A	0.392	168	0.498	230	4.3
1B	0.392	168	0.487	230	8
2A	0.544	105	0.555	160	6.9
2B	0.544	105	0.602	160	11.5
3A	0.544	105	0.527	160	8
3B	0.544	105	0.569	160	12
4A	0.544	105	0.615	160	5
4B	0.544	105	0.644	160	9.2
5A	1.15	74.5	1.47	110	5
5B	1.15	74.5	1.56	110	6.4

A- Corning, 0211, glass substrate.
B- Englehard quartz substrate.

Table VI

(Second Quarterly Report)

INDUCTOR VALUES

Substrate	Conductor width (mils)	Space (mils)	Outer diameter (mils)	Inner diameter (mils)
1	25	25	0.8	0
2	35	15	0.8	0
3	15	35	0.8	0

Substrate	Theoretical L(μh)	f_o(mc)	Actual L(μh)	f_o(mc)	Q (30 mc)
1	0.544	105	0.602	160	11.5
2	0.544	105	0.569	160	12
3	0.544	105	0.664	160	9.2

Substrate	Expected L(μh)	f_o(mc)	Q (30mc)	Actual L(μh)	f_o(mc)	Q (30mc)
1A	2.41	80	23	2.64	54	9.1
2A	2.28	80	24	2.74	57	7.9
3A	2.66	80	18.4	3.17	54	8.1

1 - Englehard quartz substrates (one-inch square and 40-mils thick).

2 - All values measured at 30 mc.

5. HIGH-PERMEABILITY FERRITE FILMS

5.1 Introduction

The investigations of vacuum-deposited, thin-film ferrites of the Fe_3O_4-B_2O_3 mixtures were performed with emphasis on the physical research as well as development of thin-film, ferrite-core inductors. Since efforts in vacuum depositing thin-film ferrites were first initiated in this laboratory, the results are still in the realm of pure physics. The application of the ferrite films as cores for thin-film inductors has not been technologically advanced to the improvement of the thin-film inductors. The results of the investigations are discussed in this section.

5.2 Structure Properties of Ferrite Films

5.2.1 Structure Evaluation

The earlier results concerning the chemical composition of the films deposited from the Fe_3O_4-B_2O_3 mixtures showed that the concentration of the impurities present in the starting mixture increased by slight amounts in the deposited films. However, the amount of elemental, or reduced, iron was measured from about 0.1% of the 90% Fe_3O_4-1% B_2O_3 mixtures. The percentage of free iron varied only with starting mixtures and not with substrate temperatures or vacuum annealing. The film structure, however, is substrate- and annealing-temperature dependent; increasing degrees of magnetite structure are developed at temperatures above 500°C.

Initial investigations of the film structures by X-ray diffraction studies reported in the first quarterly report were supplemented by electron-beam diffraction studies. The results reported here are of the 95% Fe_3O_4-5% B_2O_3 mixtures. Films that were deposited at temperatures to

500°C had glossy, smooth surfaces. Minute crystals were discernible at 600°C, with increasing growth size to 700°C. These are shown in figure 21(a and b). Films were stripped from substrates, and the structure was studied in the electron microscope. The films deposited at temperatures less than 500°C were structureless, i.e., amorphous. Films deposited on SiO-coated copper grids at thicknesses of approximately 50 Å at room temperature were studied in the electron microscope. The films were amorphous and continuous. The samples were heated in situ in the microscope, and the changes were observed as a function of temperature. The films were amorphous to 420°C, but this temperature, several scattered nuclei appeared and no significant growth was observed. The particles showed a slight tendency for an ordered structure. At 550°C, a high density of crystals formed rapidly; this is shown in figure 22. Electron transmission-diffraction patterns of elemental iron were observed at a few discrete areas. The pattern is shown in figure 23. There were no other patterns discernible. The crystal growth continued to increase, and the photomicrographs of the films at 800°C are shown in figure 24 (a and b). The electron transmission-diffraction patterns of the film at 800°C are shown in figure 25. The film is highly crystalline, and the pattern, in general, agrees with the X-ray diffraction patterns of ferrite films annealed at 750°C for 15 minutes in the vacuum system (See First Quarterly Report, figure 27).

Since Fe_3O_4-B_2O_3 mixtures were reactive with tantalum boats, and less reactive with tungsten boats, rhenium boats were fabricated and tried. The improved stability of the mixtures has not been shown at this time.

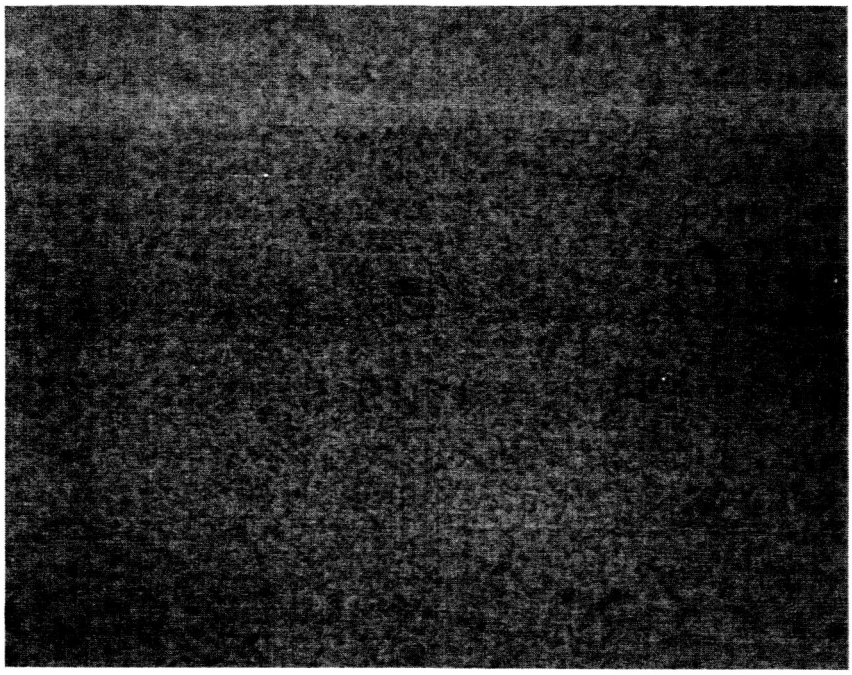

(a) E Fe_3O_4 - 49a. SUBSTRATE TEMPERATURE 600°C

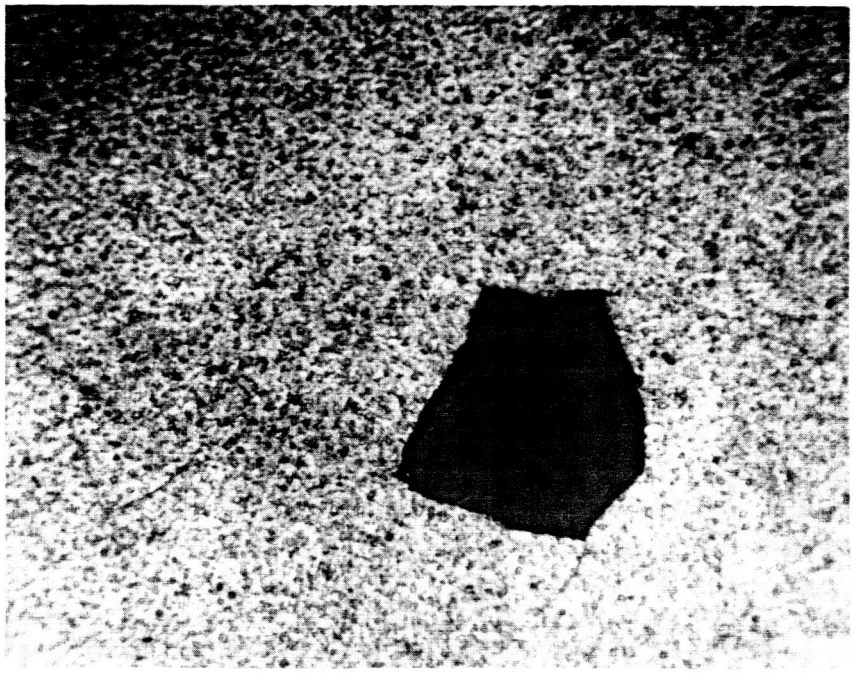

(b) E Fe_3O_4 - 42a. SUBSTRATE TEMPERATURE 700°C

Figure 21. Microphotographs of Fe_3O_4 Film at (a) 600°C and (b) 700°C

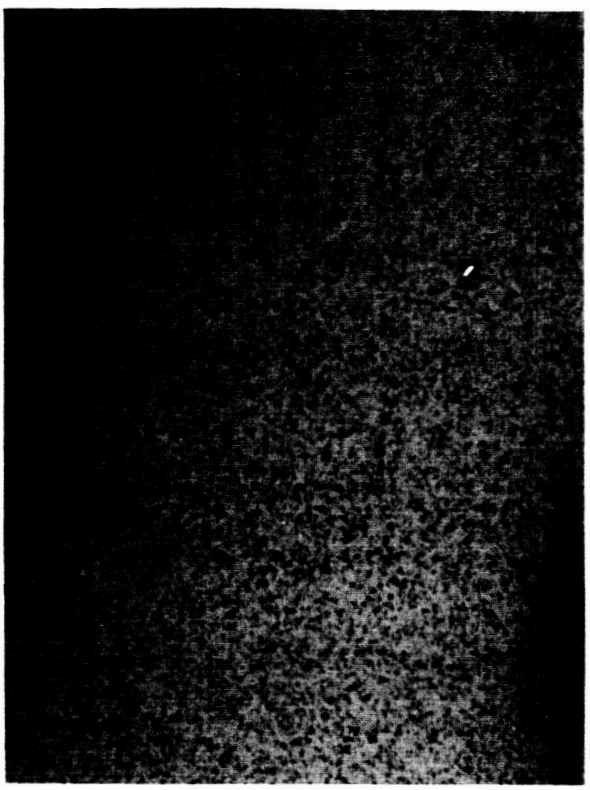

Figure 22. Nuclei Growth of Fe_3O_4 Films at 550°C

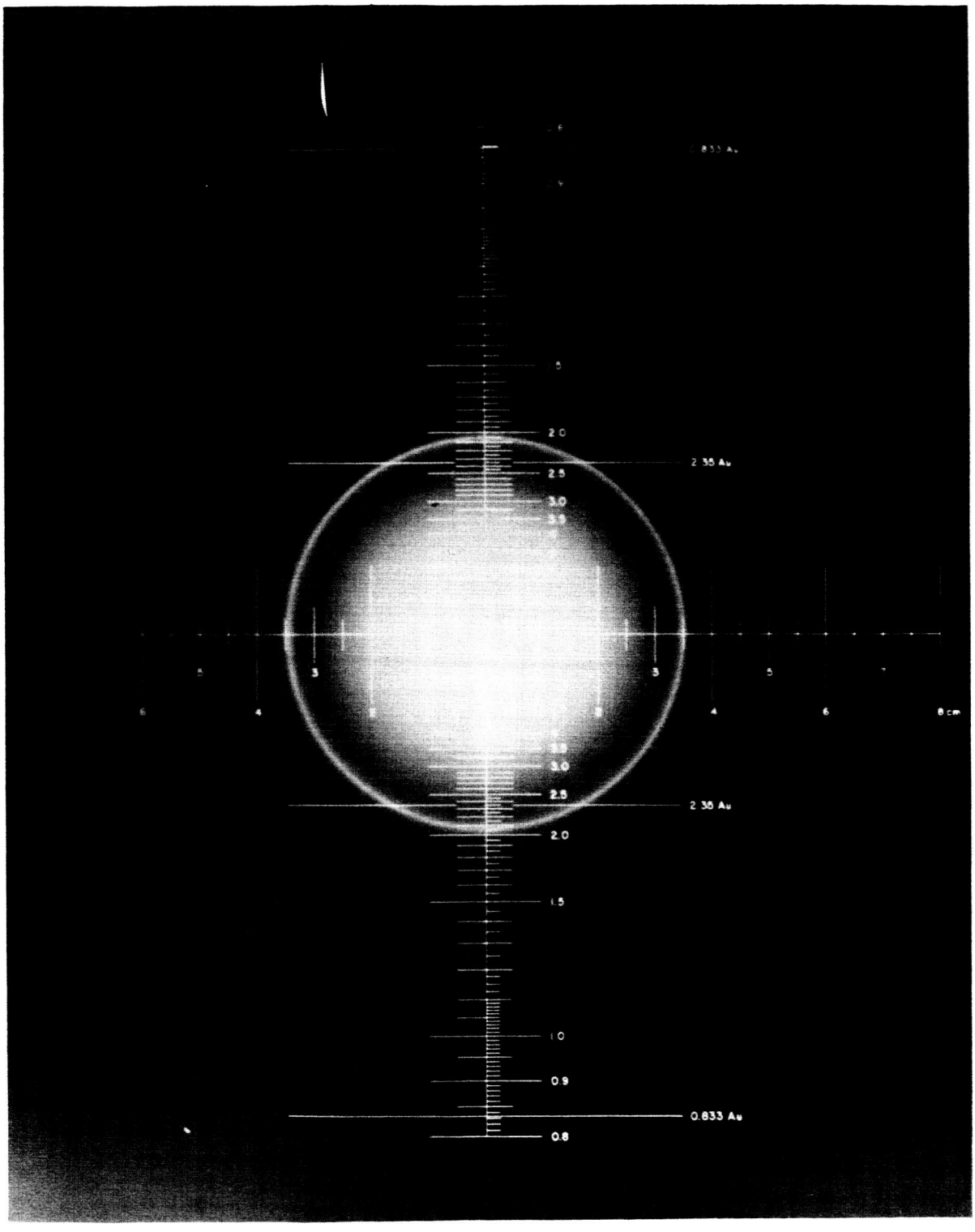

Figure 23. Electron-transmission Diffraction Pattern of Fe

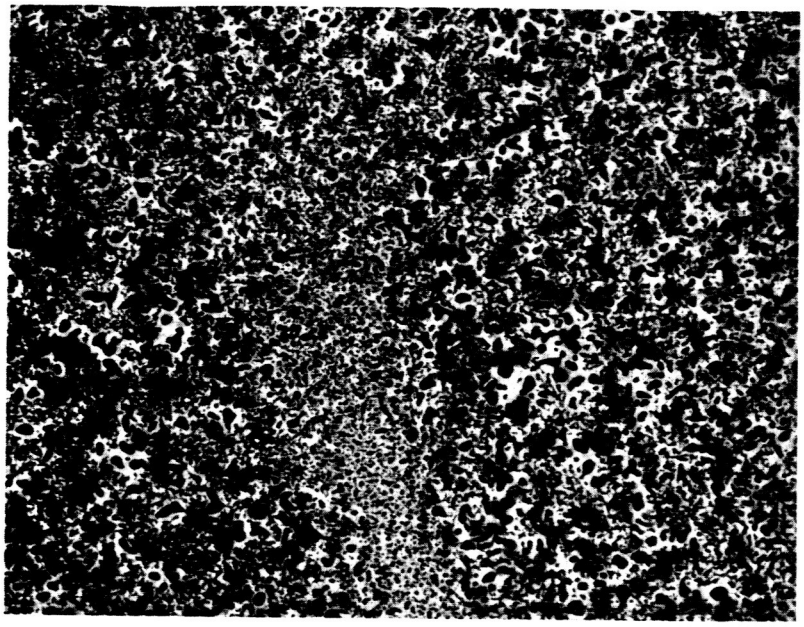

a) 4,800X

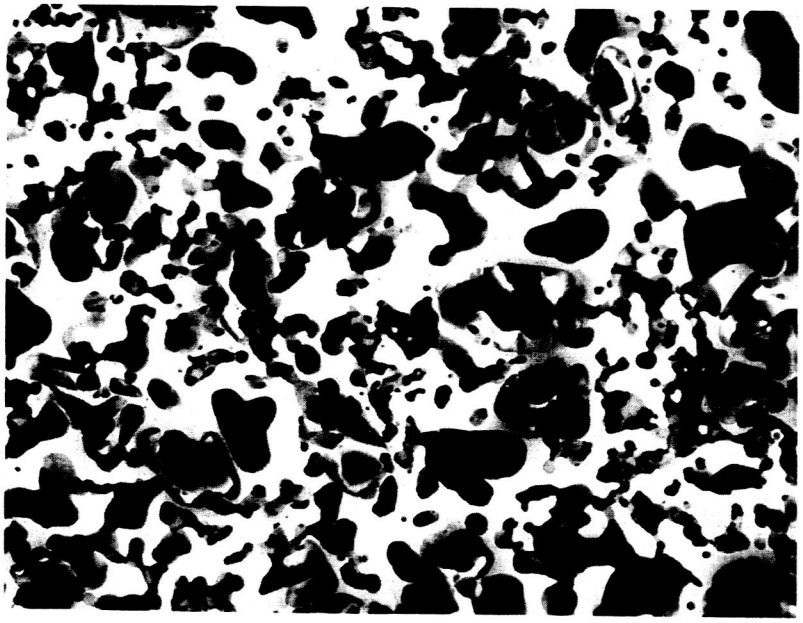

b) 35,000X

Figure 24. Microphotographs of Fe_3O_4 at 800°C

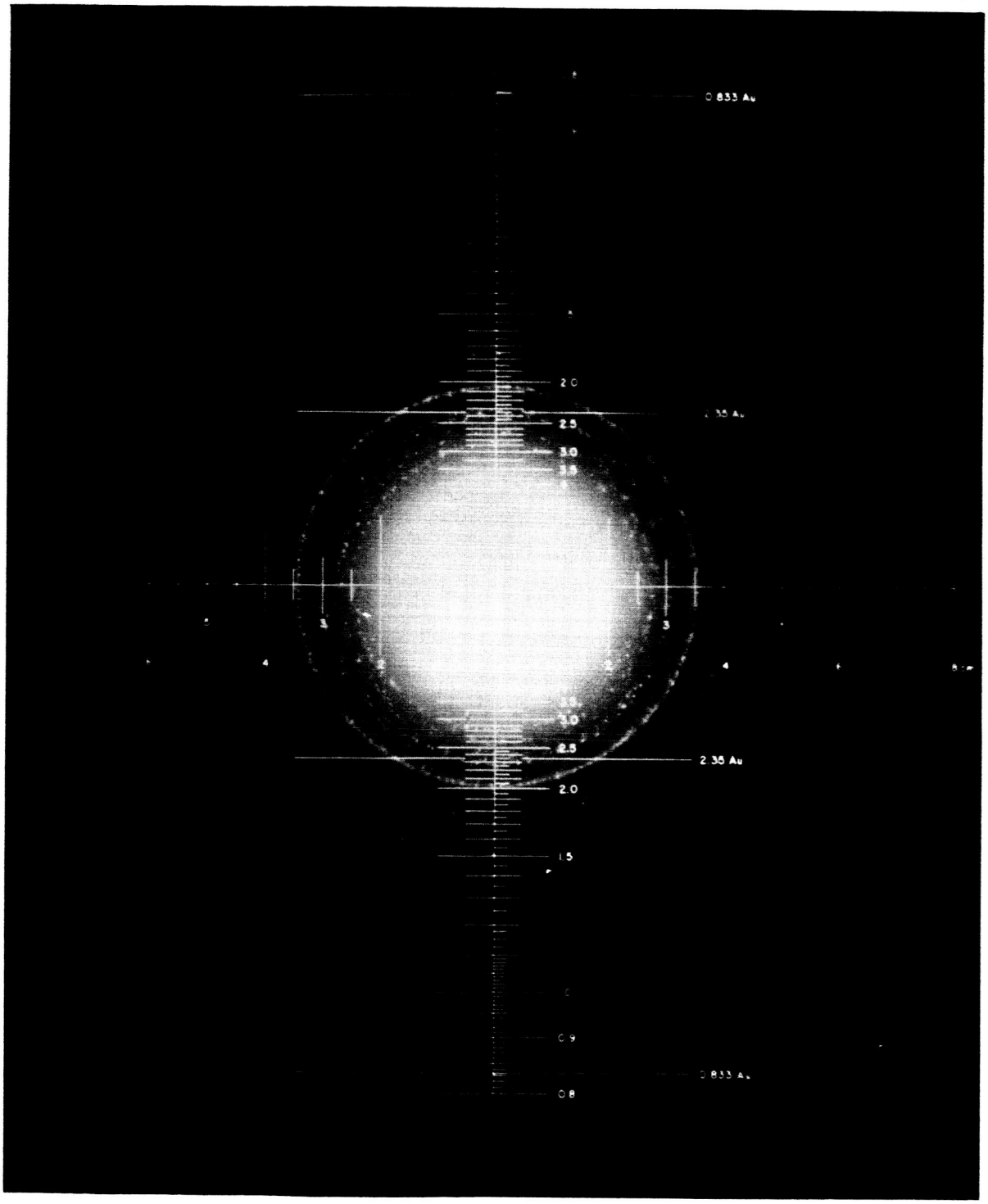

Figure 25. Electron-diffraction Pattern of Fe_3O_4 Films at 800°C

The X-ray and electron-beam diffraction studies, in conjunction with the chemical analyses, shown that Fe_3O_4 films can be vacuum deposited from tungsten boats; however, 0.1-0.3% free iron is present in the films regardless of deposition and annealing parameters.

5.3 Magnetic Properties of Thin-Film Ferrites

5.3.1 dB/dt and B-H Measurements

The magnetic-switching dB/dt peaks (unintegrated signals) and the B-H loops (integrated signals) were measured by a modified Helmholtz drive coil with a figure "8" sense coil.[6] A photograph of the equipment is shown in figure 26. The magnetic field strength of the drive coil was measured at 600 cps with a Hall-effect gaussmeter. The field, in oersteds, was linear, with drive-coil current to the maximum fields of 60 oersteds. The dB/dt peaks at 600 cps are shown in figure 27a. The switching field strength is 2.7 oersteds. The integrated signal is shown in figure 27b. The inductance, or the value of B, of the B-H loop cannot be measured directly since the vertical response to a voltage signal corresponding to the magnetic induction is not readily calculable. However, it is possible to calibrate the vertical signal, the magnetic induction in gauss, by inserting a known film value of a standard ferromagnetic film. This was done by the use of a foil of nickel 12.5 μ thick and vacuum-deposited nickel film of varying thicknesses. According to Neugebauer,[7] the $4\pi M_s$ (saturation magnetization) of the nickel in film form is the same as in bulk form. That is, the evaporation parameters do not have appreciable effects on varying the saturation magnetization, as in the case of most films. The saturization magnetization was measured to be approximately 6000 gauss.[8] This value is

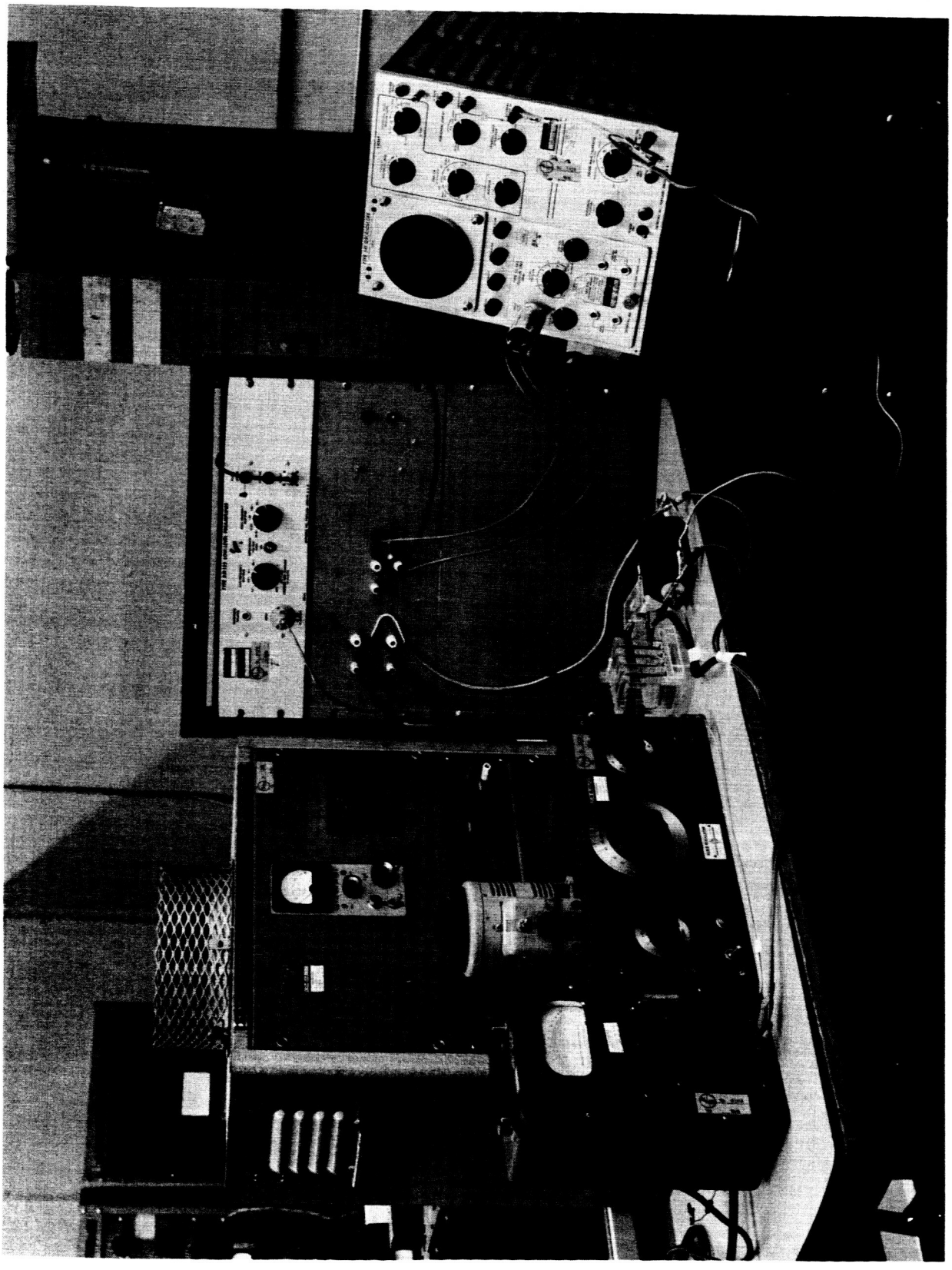

Figure 26. Electronic Apparatus for Measuring Magnetic Property of Thin Films

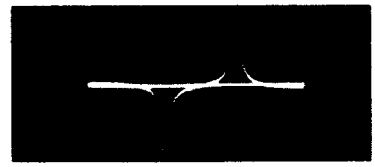

(a)

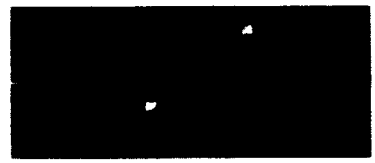

(b)

Figure 27. (a) dB/dt Peaks and (b) Integrated B-H Loop of Ferrite Films

comparable to the value for magnetite; however, the coercive field of these films is several magnitudes less than of the bulk magnitite.[9]

An important substrate dependency of the low-coercivity films has been observed. That is, the low coercive fields are present in films deposited at substrate temperatures of 300°C or less. At higher temperatures, the films are magnetic and do not switch at 60 oersteds, the maximum field of the drive coil. The correlating diffraction data indicate that the ferrite phase of the film would be present.

5.3.2 Magnetic Anistropy of Low-coercivity Films

The experimental magnetization anisotropy of the low coercive films is now described. The amplitude of the dB/dt-induced voltage peaks in the sense coil was measured as a function of angular rotation of the film in the H field. The integration of the dB/dt peaks by an electrical RC network gives rise to the B-H hystersis loops. The anisotropy field, saturization magnetization, and anisotropy constant can be readily determined from the B-H loop of uniaxial ferromagnetic films. The purpose of determining the magnetization angular dependence by the dB/dt peaks is that it was noted that the films did not exhibit uniaxial magnetic anisotropy. Changes in the unintegrated switching pulses as the film is rotated can be used in the accurate determiniation of the easy axes of the films.[10] The films were carefully positioned to obtain symmetry in the positive and negative dB/dt peaks during rotation. The plot of the peaks as a function of rotation angle is shown in figure 28. The inserts are oscilloscope traces of the dB/dt peaks at angular positions of 0°, 45°, 60°, 90°, and 120°. The zero-degree orientation of the film with respect to the applied H field was

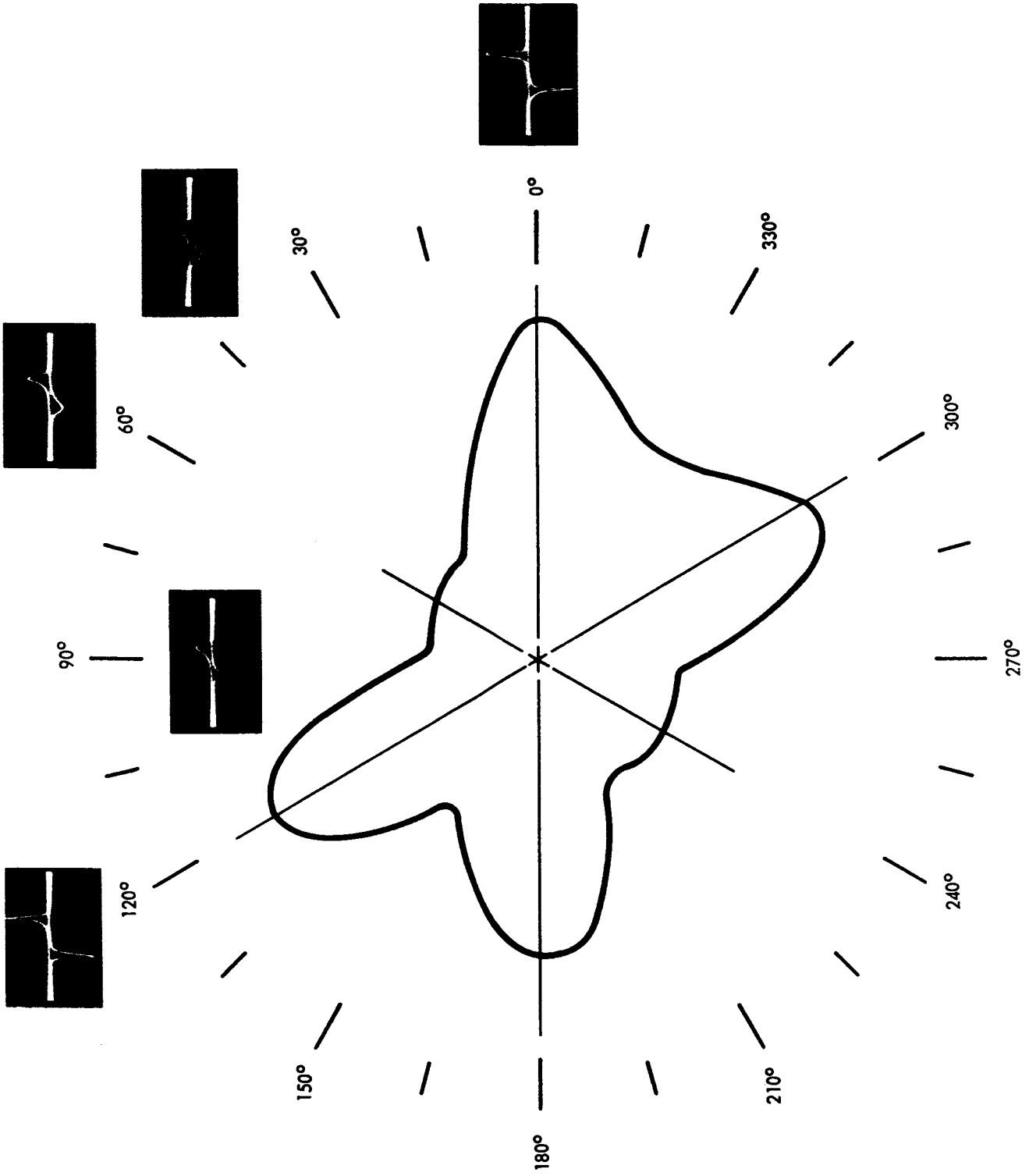

Figure 28. Plot of Average Amplitude of dB/dt Peaks as Film is Rotated in Magnetic Drive Field

determined by searching for the angular position of maximum dB/dt amplitude in the drive field.

The cusps of the magnetic orientation envelope shown in figure 28 exhibit a strong hexagonal symmetry. The cusps, axes are experimentally within $\pm 3^{o}$ of the major axes when orientated so that the strongest dB/dt amplitude is parallel to the magnetic drive field. It was found experimentally in all of the films that the position of the maximum amplitude was always parallel to the earth's magnetic field. The angular position of the minor cusps could be at either 60^{o} or 120^{o} with respect to the earth's field.

The sixfold magnetic anisotropy phenomenon was consistent for the films reported here, regardless of film geometry at substrate temperatures below $300^{o}C$.

A model describing these results can, at best, be tentative because the films do not exhibit structure of long-range order, but do exhibit magnetic anisotropy. Since the magnetization vector, i.e., directions of easy magnetization of the films, must have the symmetry of the crystal lattice,[11] it is assumed that the symmetry shown in figure 28 could be due to hexagonal crystalline structure of short-range order within the film. The cation impurities and elemental iron found in the films could be centers of such short-range-order volumes in the films. However, the same impurities, including elemental iron, are found in films that have been annealed above $500^{o}C$ and exhibit magnetite structure. To date, X-ray and electron-beam diffraction investigations have not been successful in experimentally

correlating the observed data. The origin of the well-resolved magnetization anisotropy cannot be determined at this time.

5.4 Summary for Thin-film Ferrite Material

The efforts expended in the investigation of thin-film ferrites were threefold. The first was to develop a technique by which ferrite thin films could be deposited by standard vacuum-deposition methods completely *in vacuo*. The second was to determine the magnetic properties. The third was the application of the ferrite as cores to thin-film inductors to increase the inductance.

The first phase of the investigations was highly successful. The investigations of the chemical compositions, film structures, and evaporation parameters of Fe_3O_4-B_2O_3 mixtures showed that magnetite films could be deposited utilizing vacuum-deposition techniques. The second phase of the investigations revealed that, at substrate temperatures less than 350°C, the films were amorphous and a low, coercive, ferromagnetic film existed. A sixfold magnetic anisotropy of these films was found to be predominant. At substrate temperatures above 350°C, the films showed increasing degrees of order of magnetite to a maximum temperature of 700°C. These films exhibited high coercivities of approximately 100 to 250 oersteds.

The application of the thin-film ferrites as cores in thin-film inductors did not increase the inductance of the coils. The reasons for such results are described in section 5.6.

5.5 Evaluation of Ferromagnetic Cores

5.5.1 Ferrite Core Inductors

As described in the introduction to this section, the application of

the ferrite films as magnetic cores to inductors is one of the goals of the ferrite phase. The results to date have not increased the inductance of the coils. The data presented here are experimental, and the results of the ferrite (and iron) core inductors are compared with "air" core inductors.

Since the design and techniques of fabrication of the inductors have been adequately described in section 4, description of the coils here is omitted. However, it will be stated that the single-turn indicator suffices for evaluation of the cores.

Three sets of coils were evaluated. The first set is the coil on the substrate. The second set is an SiO-coated coil on a substrate. The reason for the SiO-coated coil is that, as described in the second quarterly report, the resistivities of these ferrites (magnetite) were sufficiently low to increase the loss and effective capacitance, correspondingly decreasing the Q and inductance. The SiO film would serve as an insulating barrier between the ferrite (or iron) and the coil. The third set was the ferrite-SiO-coil laminated configuration. The Q and capacitance are measured as a function of frequency. The results are compared in table VII.

The data of table VII show that there is a slight increase of capacitance of the SiO-coated coil over the "air" core inductor (which means a slight decrease in inductance). The results could be due to the change of permeability that the inductor experiences when SiO is substituted for "air". The permeability of SiO films ranges from 5 to 6. The layer of Fe_3O_4 on top of the SiO did not increase the inductance, as determined by the fact that the capacitance increased for a given frequency. The Q of

Table VII

COMPARATIVE DATA FOR FERRITE CORE INDUCTORS

f (mc)	Coils		SiO-Coil		Fe_3O_4-SiO-Coil	
	Cap (pf)	Q	Cap (pf)	Q	Cap (pf)	Q
80	79.0	63	82.5	61	94.1	56.1
100	47.1	72	52.1	67	69.8	62
200	10.2	87	12.8	77	14.6	75
250	6.2	87	7.9	80	9.92	78

the ferrite core inductor exhibited essentially no change at the higher frequency.

Conclusion

It is not known what factors prevent an increase of inductance, even though the Fe_3O_4 is highly magnetic and film thicknesses were 15 to 20 microns. The dielectric loss may be the factor that inhibits increased inductance at these frequencies. . The resistivity of the Fe_3O_4 films is in the range of 2 ohm-cm. This is the value expected for magnetite.[12] The nickel-zinc ferrites have resistivities in the 10^{12} ohm-cm range. Therefore, it is expected that the deposition of such ferrite films should show an increased inductance for the coils.

5.5.2 Iron-core Inductors

The single-turn film inductor configuration was used to evaluate the properties of iron-core films. The deposited iron films were magnetic, as determined by a static magnetic field. However, no coercive switching was observed when the iron films were inserted in the Helmholtz coil. The B-H loop did indicate that the magnetic iron films were lossy.

The layered configuration consisted of four sets for inductor evaluation. The first set was simply the coil on a substrate. The second was the SiO-coated coil. The third was iron film deposited on the SiO-coated coil. Finally, the fourth set was as follows: An iron film was deposited on the substrate, a layer of SiO, the coil, an over coat of SiO, and, finally, a top layer of iron. The last configuration was to enhance the effect of the iron as the core for the inductors.

The Q and inductance of the four sets were measured at various frequencies. The results are shown in table VIII. The SiO-coated inductor shows a slightly smaller value of inductance when compared with the uncoated coil above. This agrees with the data concerning the ferrite core inductors. The inductance of the iron deposited over the SiO-coated coil decreased by nearly 40%. It was noted that, at 80 mc, the capacitance was greater than 110 pf; therefore, a resonance was not detected due to the limitations of the Q meter. The inductance of the coil sandwiched between the SiO and iron films decreased by more than 50%. The capacitance at 80 mc and 100 mc was too large for a resonance condition. The changes of inductance for the thin-film iron-core inductors correspond to the change, a comparable decrease, of iron in bulk forms (i.e., as a substrate).

5.6 Summary for Iron-Core Material

The iron-core evaluation proceeded as expected. The use of iron at high frequencies is limited by the eddy currents and hysteresis losses generated at such frequencies. Thus, it was proved that even very thin films of iron are not feasible as inductor cores to increase the inductance for electronic applications.

5.7 Ferrite Film Program Conclusions

The initial permeabilities of the vacuum-deposited ferrites have not been measured. This is to be done by a torque magnetometer. Instrumentation for such measurements is being procured. However, by comparison of the dB/dt peaks of the low-coercivity ferrite films with nickel films, an estimate of the "dynamic" permeability can be made. The initial permeability of nickel is 1120. The initial slope of the dB/dt peaks of the ferrite

Table VIII

COMPARATIVE DATA ON IRON CORE INDUCTORS

f (mc)	Coil		SiO-Coil		Fe-SiO-Coil		Fe-SiO-Coil-SiO-Fe	
	Q	Ind. (μh)	Q	Ind. (μh)	Q	Ind. (μh)	Q	Ind. (μh)
80	54.5	0.041	54.0	0.039	--*	--	--*	--
100	81.5	0.042	75.0	0.039	20	0.026	--*	--
200	101.5	0.042	86.0	0.040	34	0.026	15.5	0.020
250	105.0	0.043	102.5	0.041	48	0.026	21.0	0.020

*No measured resonance value.

is approximately twice as large; therefore, an estimated value for the permeability of these films is 2000.

This indicates that the inductance of a thin-film coil should be increased, by a factor of 10-100, by the replacement of the "air" core with the ferrite core. There are two factors that must be taken into consideration for successful operation at the 80-300 mcs region.

The first is that the films must be of higher resistivity, and the second is that the frequency response of the films must be evaluated. The first factor can be readily annealed by varying the ferrite composition. Nickel-zinc and nickel-iron ferrites have resistivities of 10^6 and 10^9 ohm-cm, respectively. The loss tangent of nickel-iron ferrite is extremely low at 10^5 c/s. The permeabilities of these ferrites are in the range of 200-300. However, such films are capable of being incorporated in the thin-film inductor task by increasing the film thickness from 20 microns to approximately 100 microns.

The success of vacuum depositing thin-film ferrites (Fe_3O_4) exhibiting magnetic properties comparable to the bulk ferrite (Fe_3O_4), with the exception of several anomalies noted, should warrant further investigation of other metal-composition ferrites.

6. CIRCUIT-DESIGN CONSIDERATIONS

6.1 Introduction

Work on potential circuit-design concepts for the TFPCTS has been underway for most of the time since the inception of this contract. The purpose of this work has been to facilitate the design phase of this equipment by introducing the circuit-design engineers to monotronics.

6.2 Passive Component Requirements

Minimum specifications for passive components to be used on this project are given below. These specifications are tentative, and are based on the present system-design concept.

6.2.1 Typical Value Components

Utility Resistors: 100 ohms to 1 megohm, ± 20% initial tolerance, 0.10-watt power rating, frequency response flat to 10 mcs.

Precision Bias Resistors: 50K to 1 megohm. A bias voltage stability of 1% requires a resistance ratio stability of 0.5% ratio. This stability must hold over a 0° to 50°C temperature range.

Utility Capacitors: 10 pf to .005 μf, ± 20% initial tolerance, 20 V breakdown. Frequency response flat to 10 mcs.

Precision RC Networks: Nominal R value = 10 K; Nominal C range = 0.001 to 0.005 μf; RC product initial tolerance or trimmed tolerance must be better than 0.3% including temperature deviations.

Tapered RC Networks: These networks may be used for harmonic suppression of VCO outputs. Attenuation specifications for the second and third harmonics are 30 db and 60 db.

High Frequency Resistors and Capacitors: Resistance less than 5 K ohms, capacitance 1 to 100 pf. Both types of components should be usable to 300 mcs. Capacitors should have high Q.

Coils for RF: .01 to 0.2 μ henry. Q greater than 30 to be used for R-F circuitry from 100 to 300 mcs.

6.2.2 Large-value Components

Components which would be useful if available.

Capacitors: Large values for power supply and audio output, greater than 10 μf.

Inductors and Transformers: For 30 mc IF, Q greater than 30, L probably in the range of .5 μh to 50 μh.

Inductors and Transformers: Very large values for power supply and audio frequencies, L greater than 0.1 henries.

6.3 Passive Component Discussion

Recently, Melpar has prepared a brochure, "Characteristics of Evaporated Thin-Film Circuits," which is included as an appendix to this report. This brochure gives a very detailed report of thin-film passive components in all aspects, except frequency response.

The values, tolerances, temperature characteristics, and frequency responses given in section 6.2.1, Typical Value Components, probably can be attained in thin-film form with reasonable yield figures in a usable substrate area. The major specifications are stated in considerable detail in the brochure. Most value and configuration thin-film resistors have a flat frequency response to 10 mcs. Small value, short resistors have a flat frequency response beyond 250 mcs. 250 mcs is the limit of the test

equipment used in resistor-frequency evaluations that have been made. The precision and tapered networks will be low-yield products, but seem feasible.

The large-value components, given in section 6.2.2, have only a limited possibility in thin-film form. For example, multilayer capacitors can be formed with a value of one microfarad per square inch. The question raised is: "Even though large capacitance values can be formed, would it be feasible to use a large number of substrates to achieve large values of capacitance?" Probably, one small discrete component capacitor would be preferable.

7. CONCLUSIONS

Practical techniques have been developed to make a thin-film triode with a promising configuration for high-frequency performance. These methods are now being employed in the fabrication of devices. Work on the selected semiconductor materials will continue because perfection in the formation of semiconductor films for optimum field effect is, of course, always a necessary goal. The metal-base transistor is currently at the stage of development where attempts to form junctions, back to back, with reverse blocking direction are being made. In other words, the solution of the physical problem of compatible deposition of two diodes, one on top of the other, is presently being worked out. The diodes themselves are being tested for a thorough investigation of the mechanisms of operation to design them for high-frequency operation and varactor usage. The inductors have proved to be a useful circuit-design component. The Thin-Film Ferrite Investigation has come to a close for the present because the work effort has already exceeded the time and man-hours allocated for this investigation on the original PERT Chart. These films seem to prove that ferrites can eventually be deposited using only standard vacuum-deposition techniques. Thin films of iron, unfortunately, maintain the bulk iron properties which prevent its use at high frequencies. As shown on the PERT Chart, work on the possibility of forming a transformer in the coming quarter will be attempted. The potential exists for useful coupling between coils through the air (or vacuum), or through a substrate.

8. REFERENCES

1. T. Ichimiya, T. Niimi, K. Mizuma, O. Mikami, Y. Kamiya, and K. Ono, "Solid-State Physics in Electronics and Telecommunications," Proc. of Intl. Conf., Brussels, June, 1958, Vol. 2, Semiconductor, Part 2, p. 845-853.
2. P. P. Konovov and I. B. Shevchenko, Soviet Physics--Solid State, 2, 1027 (1960).
3. D. A. Jenny and R. H. Bube, Physical Review, Vol. 96, No. 5, Dec. 1, 1954, p. 1190.
4. R. Glanz, J. G. Kren and W. J. Patrick, Journal of the Electrochemical Society, Vol. 110, No. 5, May 1963, p. 407.
5. R. H. Bube, Photoconductivity of Solids, John Wiley and Sons, Inc., 1960, p. 174.
6. "Memory Study and Development Program," Final Report on Contract No. AF 30(635)-1401, 1959.
7. C. A. Neugebauer, "The Saturization Magnetization of Nickel Films of Thickness Less than 100 Å," The Structure and Properties of Thin Films, Edited by C. A. Neugebauer, et al., John Wiley and Sons (1965).
8. J. Smit and H. P. J. Wijn, Ferrites, J. M. Wiley and Sons, Printed in The Netherlands) 1959, p. 157.
9. A. Baltz, "Preparation of Ferrite Films by Evaporation," Appl. Phys. Letters, 7, 10 (1965).
10. J. B. Goodenough and D. O. Smith, "The Magnetic Properties of Thin Films," MIT Technical Report No. 197 (1959).
11. J. Smit and H. P. J. Wijn, Op. Cit., Chapter IV.
12. Ibid., p. 235.

Senior personnel who participated in work on this contract this quarter are:

Dr. Charles Feldman

Mr. Charles E. Gane

Mr. William A. Gutierrez

Mr. Michael Hacskaylo

Mr. John C. Mould

Mr. Wendell Spence

Mr. Barry J. Weiner

Mr. Herbert L. Wilson

Prepared by:

Barry J. Weiner
Liaison Project Engineer

Approved by:

Charles Feldman, Manager
Physical Electronics Laboratory

E. L. Ditz, Manager
Space Research and Technology Center

Paul E. Ritt, Vice President
Research and Engineering

APPENDIX

"Thin-Film Circuits"

CHARACTERISTICS OF EVAPORATED

THIN FILM CIRCUITS

The following six tables describe the performance characteristics of evaporated thin film rhenium resistors, borosilicate capacitors, "air core" inductors, conductors, etched chromium resistors, terminals for welded or soldered wire connections, and substrate materials.

Similar data describing thin film diodes, triodes, typical hybrid and monotronic circuits are scheduled for November 1965 release. Also, performance data in general will be revised periodically to reflect improved processes and cumulative test data.

MELPAR INC
A SUBSIDIARY OF WESTINGHOUSE AIR BRAKE COMPANY

7700 ARLINGTON BOULEVARD, FALLS CHURCH, VIRGINIA 22046
AREA CODE 703
JEFFERSON 4-6000

TP5-415/10

TABLE I

THIN FILM RESISTORS

Materials: Re resistors with SiO protective coating and Cr, Cu, Au, or Al terminals.

Range:

100 to 20,000 ohms/sq.

10 ohms to 160 megohms/sq. inch for masked depositions

10 ohms to 40,000 megohms/sq. inch for photoetched films

Tolerance (at 10,000 ohms/sq. without trimming):

± 20% for 90% yield

± 5% for 50% yield

Tighter tolerances/higher yields at lower sheet resistances. (Thermal trimming can be used.)

Maximum Temperature:

400°C continuous in room ambient air (for Au or Al surface films on terminals).

Temperature Coefficient of Resistance (TCR): (Average TCR for temperature between 25°C and 125°C.)

± 50 ppm for 100 to 300 ohms/sq.

- 100 ppm ± 5% at 600 ohms/sq.

- 200 ppm ± 5% at 4300 ohms/sq.

- 340 ppm ± 5% at 10,000 ohms/sq.

Shelf Life:

Less than 1% change in resistance up to 11,000 ohms/sq. over a 4.5-year period -- typical.

Age Stability Under 60 cps ac Load:

Less than 0.5% change in resistance of 500 ohms/sq. resistors after 5000 hours of operation at 65° to 75°C substrate temperature in room ambient air. (Approximately 0.25 watt dissipation for each of 10 resistors per substrate -- up to 200 watts/sq. inch of resistor area.)

Voltage Effects:

0.27% reduction in 11.15 megohms (7250 ohms/sq.) resistor from 0 to 825 volts dc.

VCR = - 3.32 ppm/volt -- typical.

Current Noise:

Noise index equals - 8 db (0.4 μv/v) for 18.7 megohms (10,570 ohms/sq.) resistor -- typical.

TABLE II

ETCHED THIN FILM CHROMIUM RESISTORS

Range:

50 to 10,000 ohms/sq
5 ohms to 100 megohms/sq inch for mask deposition
5 ohms to 20,000 megohms/sq inch for photoetched films

Tolerance at 500 ohms/square, for photoetched films:

Without Trimming:	±15% for 90% yield, overall
	± 5% for 60% yield per resistor
With Trimming:	±1% for 95% yield per resistor
	±0.1% for 60% yield per resistor

Maximum Temperature in Room Ambient Air:

200°C

Temperature Coefficient of Resistance (25° to 125°C):

250 ohms/sq	±20 ppm
500 ohms/sq	- 100 ppm

Shelf Life:

Less than 0.5% change in resistance over a one-year period.

TABLE III

THIN FILM CAPACITORS

Materials and Configuration: Borosilicate dielectric aluminum plates; single dielectric layer.

Range:

3,000 to 15,000 pf/cm^2

19,350 to 96,750 pf/in^2

0.5 pf minimum for smallest practical masked area

Tolerance:

$\pm$ 8% overall

General Equations:

$$\frac{C}{A} = 8.87 \times 10^6 \frac{e}{d}$$

$$V_w = Kvd = 8.87 \times 10^6 \frac{eKv}{C/A}$$

where C = capacitance, pf = $\mu\mu f$

A = capacitor area, cm^2

e = dielectric constant

d = dielectric thickness, Å

V_w = withstanding voltage (continuous), volts dc

Kv = dielectric strength, volts/Å

Dielectric Constant:

e = 4

Dielectric Strength and Withstanding Voltage:

$Kv \geq$ 0.03 volt/Å = 3×10^6 volts/cm

This is for a continuously applied voltage, where no degradation occurs. A continuous voltage about 28% higher results in a reduction in dc resistance which stabilizes after about 30 minutes of application. A voltage about 43% higher results in catastrophic breakdown after about 10 seconds of application.

For the above values and range, $V_w = 0.03d = \frac{1.065 \times 10^6}{C/A}$ volts or V_w increases from 71 to 355 volts dc and C/A decreases from 15,000 to 3,000 pf/cm^2 as d increases from 2,360 to 11,800 Å.

TABLE III (CONTINUED)

THIN FILM CAPACITORS

DC Resistance:

Resistance decreases exponentially with increasing voltage. For a 15,000 pf/cm^2 capacitor, where d = 2360 Å, a typical relation is:

$$R = \frac{2.9 \times 10^{12}}{A} e^{-0.1638\, v},\ v \leq 70 \text{ volts}$$

where

R = resistance, ohms

A = capacitor area, cm^2

v = voltage across plates, volts dc

For the above example,

R = 21,500 megohms when

v = 30 vdc and A = 1 sq cm

Resistance is greater for thicker dielectric films; or as C/A decreases.

Q vs. Frequency:

Capacitor Q is defined as $\frac{Z \text{ imag}}{Z \text{ real}}$

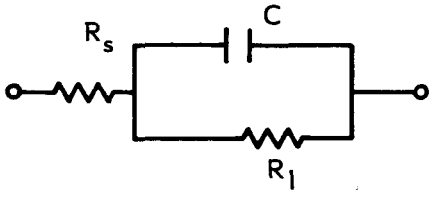

The flat plate capacitor equivalent is:

$$Q = \frac{(R_l C)\omega}{R_s R_l C^2)\, \omega^2 + \frac{(R_l C)\omega}{Q'} + \frac{(1 + R_s)}{R_l}}$$

where

C = capacitance (farads)

R_l = dc resistance of dielectric (ohms)

R_s = resistance of leads and plates (ohms)

Q' = maximum Q (determined experimentally)

ω = frequency, rad/sec ($\omega = 2\pi f$)

TABLE III (CONTINUED)

THIN FILM CAPACITORS

(Normally $R_s/R_l << 1$ and may be neglected.)

$Q' = Q_{max}$ = 100 to 1000, typical

Example:

If C = 100 pf, R_l = 10,000 megohms, R_s = 0.1 ohm, Q' = 100, and $\omega = 10^9$ rad/sec (f = 159 mc),

then Q = 99

Plate and Terminal Resistance:

$$R = \frac{\rho}{d}\frac{L}{W} = R'\frac{L}{W}$$

where

R = resistance, ohms

R' = sheet resistance, ohms/square

L = length of conductor

W = width of conductor

ρ = resistivity of conducting film

d = thickness of conducting film

$R' \leq$ 0.1 ohm/square

Humidity Effects:

No measurable changes after immersion in water for a minimum of 24 hours.

Temperature Coefficient of Capacitance:

TCC $\leq$ 100 ppm/°C for $+25 \leq T \leq +125$°C

Maximum Operating Temperature:

400°C

TABLE IV

THIN FILM INDUCTORS

Materials and Configuration: The inductors described below have a flat, two-dimensional, square, spiraling-coil configuration. They consist of one layer and do not contain any magnetic "core" materials. The conducting films generally consist of a copper film about 20,000 Å thick, deposited over a chromium film about 500 Å thick. Copper is used because of its low resistivity, high deposition rate, low cost, and compatibility with either soldered or welded joints; and chromium is used to provide strong adherence to the substrate.

Magnetic films deposited on both sides of the coil should increase the inductance in direct proportion to their permeability; deposition of magnetic films is in the research stage of development, therefore no data is furnished on them at this time.

General Equations:

$$L = 18 \times 10^{-8}\, aN^{5/3} \log 8\frac{a}{c}$$

$$a = \frac{A + B}{4}$$

$$c = \frac{A - B}{2}$$

$$N_{max} = \frac{A}{2(x + y)}$$

$$\ell = 4N\left[A - N(x + y)\right] - \frac{x}{2} + (4N - 1)y$$

$$\text{If } N = N_{max} = \frac{A}{2(x + y)}$$

$$\ell = 2NA - \frac{x}{2} + (4N - 1)y$$

$$f_o = \frac{947 \times 10^6}{\ell}$$

$$Q = \frac{2\pi fL}{R}$$

$$R = \frac{\rho}{d}\frac{\ell}{x} = R'\frac{\ell}{x}$$

where

L = inductance (henrys)

N = number of turns

A = length of longest side at the outer periphery (inches)

B = length of shortest side at the inner periphery (inches)

x = conductor width (inches)

y = distance between adjacent conductors (inches)

ℓ = total length of coil--conductor (inches)

TABLE IV (CONTINUED)

THIN FILM INDUCTORS

f_o = self-resonant frequency (cps)

Q = quality of the inductor

R = resistance of coil--conductor (ohms)

ρ = resistivity of conductor film (ohm-angstrom)

d = thickness of conductor film (angstroms)

R'= sheet resistance of conductor film (ohms/square)

Note: Changes in resistance, and therefore Q, as a function of frequency due to "skin effect" or other phenomena are neglected in the above equations. Typical thin film inductors have exhibited 12.5% to 23.4% increases in resistance as frequency increases from 0 to 30 mc. This is considerably less than is found in wire-wound inductors. Studies are being made to determine equations relating resistance and inductance to frequency and geometry of thin film inductors.

Characteristics of two typical thin film inductors are listed below. The outer dimensions, A, and sheet resistance, R', are the same for each inductor.

R' = 0.01 ohm/sq.	R' = 0.01 ohm/sq.
A = 0.6 inch	A = 0.6 inch
x = 0.010 inch	x = 0.050 inch
y = 0.010 inch	y = (not applicable)
N = 13 turns	N = 1 turn
L = 1.5 μ h	L = 0.064 μ h
f_o = 50 mc	f_o = 400 mc
Q = 16 at 30 mc	Q = 30 at 100 mc

Range and Tolerance for Masked Depositions:

Range	Tolerance
A 0.030 inch min	$\pm$ 0.001 inch
B 0.010 inch min	$\pm$ 0.001 inch
x 0.005 inch min	$\pm$ 0.001 inch
y 0.010 inch min	$\pm$ 0.001 inch
R' 0.010 ohm/sq. min	$\pm$ 10%

Typical Inductor Tolerances:

L $\pm$ 1%

f_o $\pm$ 1%

Q $\pm$ 10%

TABLE V

THIN FILM CONDUCTORS AND WIRE CONNECTIONS

MATERIALS, STARTING AT SUBSTRATE	SHEET RESISTANCE RANGE (TYPICAL) OHMS/SQ	WIRE LEADS AND JOINTS
Cr	10 to 100	welded Au or Al
Al	1 to 0.1	welded Au
Cr, Au	1 to 0.1	welded Au or Al
Cr, Cu	0.1 to 0.01	welded Au or Al, or soldered Cu
Cr, Cu, Au	0.1 to 0.01	welded Au or Al; or soldered Cu

Notes:

1. Cr and Al films have strong adherence to glass, quartz, or glazed alumina substrates, whereas Cu or Au films do not. Therefore, Cu or Au are deposited over a thin Cr adherence film. Au is used where oxidation must be minimized, particularly for high-temperature applications. Cu is used for high conductivity at low cost and for solder joints. Al has the advantage of forming a thin surface oxide which is stable up to about 500°C in air, except where the Al is in contact with certain dissimilar metals such as Au.

2. Typical wire diameters are 0.001 to 0.010 inch for welded joints and 0.001 to 0.030 inch for soldered joints.

3. Minimum thin film terminal size is 0.015 inch square for welded leads and 0.050 inch square for soldered leads.

4. Pull strength is limited by wire strength when pulled parallel to film surface for welded joints or in any direction for soldered joints.

5. Welded joints are made employing the parallel gap resistance welding technique.

6. Solder joints are generally made using ordinary lead-tin solder with a very small quantity of white resin flux. Where a thin gold surface film is deposited over the copper film and gold plated copper wire is used, oxidation at the joint is minimized and the flux may be omitted. Even where gold is used, however, the flux facilitates soldering. A small percentage of silver in the solder is necessary to prevent dissolving of the gold. An economical technique for assembling and soldering hybrid thin film circuits in quantity production lots has been developed at Melpar. The film deposition and soldering processes are controlled to the point that component leads can be unsoldered and resoldered without damage to the thin film terminals.

TABLE VI

SUBSTRATES

CHARACTERISTIC	UNITS	FUSED SILICA, CORNING 7940	ALKALIZINK BOROSILICATE GLASS, CORNING 0211	BARIUM ALUMINO SILICATE GLASS, CORNING 7059	UNGLAZED ALUMINA, AMERICAN LAVA AlSiMag614	LEAD BOROSILICATE GLAZED ALUMINA, AMERICAN LAVA GLAZE 743 ON AlSiMag614
DC Surface Resistivity at 25°C (Sheet Resistance) and 100% R.H.	ohms/sq	$\sim 10^{10}$	$\sim 10^{10}$	$\sim 10^{10}$	----	10^{10}
DC Volume Resistivity at 25°C	ohm-cm	$\sim 10^{19}$	$\sim 5 \times 10^{19}$	$\sim 10^{21}$	$> 10^{14}$	----
Dielectric Constant at 25°C + 1 mc	----	3.9	6.6	5.8	9.1	8.9
Thermal Conductivity at 25°C	$\frac{cal/sec}{cm\ °C}$	0.002 to 0.004	0.002 to 0.004	0.002 to 0.004	0.084	0.002 to 0.004
Total Emissivity at 25°C	----	~ 0.93	~ 0.94	~ 0.94	~ 0.75	~ 0.94
Thermal Expansion at 25°C (Linear Coefficient)	$\times 10^{-6}$ /°C	0.56	7.2	4.5	6.4	~ 6.4
Strain Point	°C	990	502	613	1550 Safe Temp.	700 Safe Temp.
Annealing Point	°C	1050	542	650	----	----
Softening Point	°C	1580	720	872	----	725
Density	gm/cc	2.20	2.57	2.76	3.70	----
Hardness (Mohs' Scale)	----	7	5 to 7	5 to 7	9	5 to 7
Surface Finish (Typical)	µ inches rms	----	< 0.25	< 0.25	----	< 1
Flatness (Typical)	inches	± 0.00055	±0.0004	±0.0004	----	±0.0015
Tensile Strength, 25°C	psi	1,000 to 10,000	1,000 to 10,000	1,000 to 10,000	25,000	----
Modulus of Elasticity 25°C	$\times 10^6$ psi	10.5	9 to 10	9 to 10	----	----
Poisson's Ratio 25°C	----	0.18 to 0.22	0.18 to 0.22	0.18 to 0.22	----	----
Impact Resistance 25°C Charpy, A.S.T.M. Test No. -D116 -61T	inch - lb	----	----	----	7	----
Alkali Content	%	----	----	~ 0	----	~ 3

SIZES: The production facility can handle substrates ranging in size from 0.125 x 0.250 inch to 4.188 x 4.188 inches with thicknesses from 0.010 to 0.250 inch.

Typical sizes are 1 x 1 inch and 2 x 2 inches with thicknesses of 0.010, 0.020, 0.030, and 0.040 inch.

Typical tolerances are ± 0.5% to ± 1% for 1 to 2 inch dimensions and ± 10% to ± 20% for thicknesses.